

The photocatalytic H₂O₂ production by metal-free photocatalysts under visible-light irradiation



Xiahong Xu ^{a,c}, Yan Sui ^a, Wentong Chen ^a, Wei Huang ^a, Xiaodan Li ^a, Yuntong Li ^a, Dongsheng Liu ^a, Shuang Gao ^a, Wenxin Wu ^a, Changwang Pan ^a, Hong Zhong ^{a,*}, He-Rui Wen ^c, Meicheng Wen ^{b,*}

^a Key Laboratory of Coordination Chemistry of Jiangxi Province, School of Chemistry and Chemical Engineering, Jinggangshan University, Ji'an, Jiangxi 343009, China

^b Guangdong-Hong Kong-Macao Joint Laboratory for Contaminants Exposure and Health, Guangdong Key Laboratory of Environmental Catalysis and Health Risk Control, School of Environmental Science and Engineering, Institute of Environmental Health and Pollution Control, Guangdong University of Technology, Guangzhou 510006, China

^c School of Chemistry and Chemical Engineering, Jiangxi University of Science and Technology, Ganzhou, Jiangxi 341000, China

ARTICLE INFO

Keywords:

Metal-free photocatalysts
Photocatalysis
Hydrogen peroxide
Visible light
Heterogeneous catalysis

ABSTRACT

The photocatalytic H₂O₂ production from H₂O and O₂ over organic polymers is a promising approach to achieve solar-to-chemical energy conversion. The continuous efforts have led to rapid development of various metal-free-based photocatalysts for specific H₂O₂ production, but generalizations and summarization are obviously inadequate. This review mainly focuses on the state-of-the-art development process of metal-free-based photocatalysts for photocatalytic H₂O₂ production via combining O₂ reduction and H₂O oxidation reactions under visible light irradiation. The representative research work on photocatalytic H₂O₂ production by various metal-free-based photocatalytic systems, including graphite carbon nitride (g-C₃N₄), covalent organic frameworks (COFs), covalent triazine frameworks (CTFs) and covalent organic polymers (COPs) was highlighted. The strategies for structure and property optimization of metal-free-based photocatalysts at molecular-level have been proposed for improving the photocatalytic performance. The challenges and future directions have also been provided to guide the design and synthesis of metal-free-based photocatalytic system.

1. Introduction

Hydrogen peroxide (H₂O₂) is one of the most important chemicals in the world today, which possesses satisfactory activity, strong oxidation and high energy density [1–3]. More importantly, the decomposition products of H₂O₂ are only water and oxygen, causing no secondary pollution [4,5]. It is widely used in chemical industry, environmental protection, disinfection, medicine and aerospace and other fields [6–10]. With the demand increasing, it has been attracted more and more attention for the development of efficient technology for H₂O₂ preparation [11,12]. However, the industrial production of H₂O₂ still relies on the traditional anthraquinone process [1,13], and its production goes through a series of processes such as hydrogenation and oxidation of anthraquinone, as well as subsequent extraction, purification and concentration etc. [14,15], which inevitably ties to the complex technology, high energy consumption and serious environmental

pollution [16]. In addition, the hydrogenation reaction stage requires the use of noble-metal-based catalysts and high-pressure H₂, which not only increases the cost of H₂O₂ preparation, but also brings many safety risks [17–20]. Therefore, it is a pressing requirement to develop an efficient, safe, green and sustainable method for H₂O₂ preparation.

The photocatalytic H₂O₂ production from H₂O and O₂ by using solar energy as energy input is considered to be a green, safe and sustainable H₂O₂ synthetic approach [21–25], but performance is inevitably tied to the overall properties of photocatalyst. Generally, the photocatalysts should have appropriate band structure and band gap width to enable photo-generated electrons/holes to reduce O₂ and oxidize H₂O [22]. Meanwhile, their conduction band (CB) edge must be more negative than the reduction potential of O₂, and the valence band (VB) edge should be more positive than the oxidation potential of H₂O [25]. On the other hand, the band gap of the photocatalysts should not be too wide, as this would limit their efficient use of sunlight [26,27]. Given the two

* Corresponding authors.

E-mail addresses: zhonghbush@jgsu.edu.cn (H. Zhong), meicheng.wen@gdut.edu.cn (M. Wen).

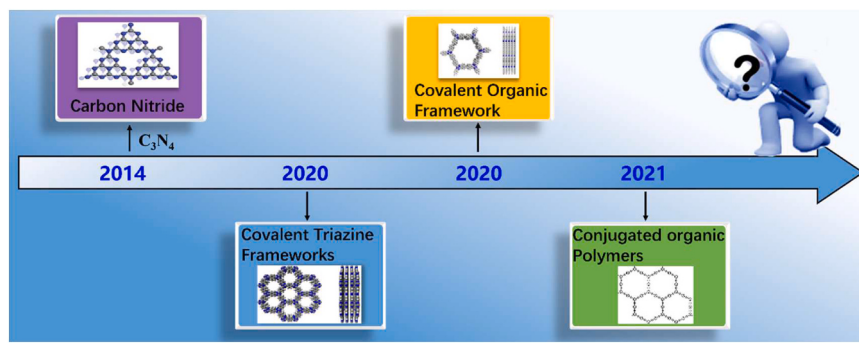


Fig. 1. The timeline of representative metal-free-based photocatalysts for photocatalytic H_2O_2 production.

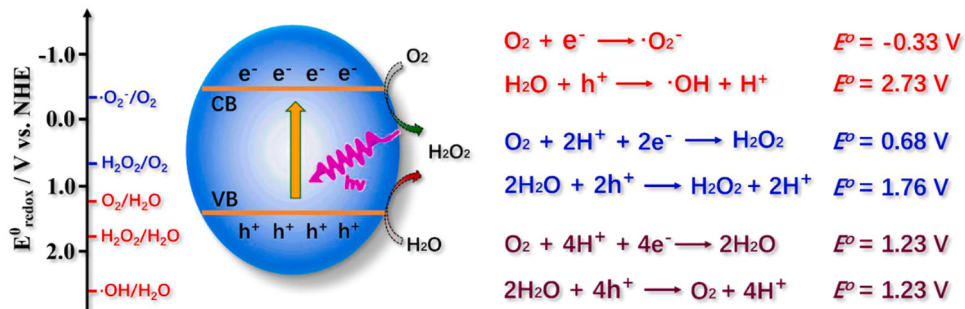


Fig. 2. Schematic illustration of the processes involved in photocatalytic H_2O_2 production and corresponding energy diagrams.

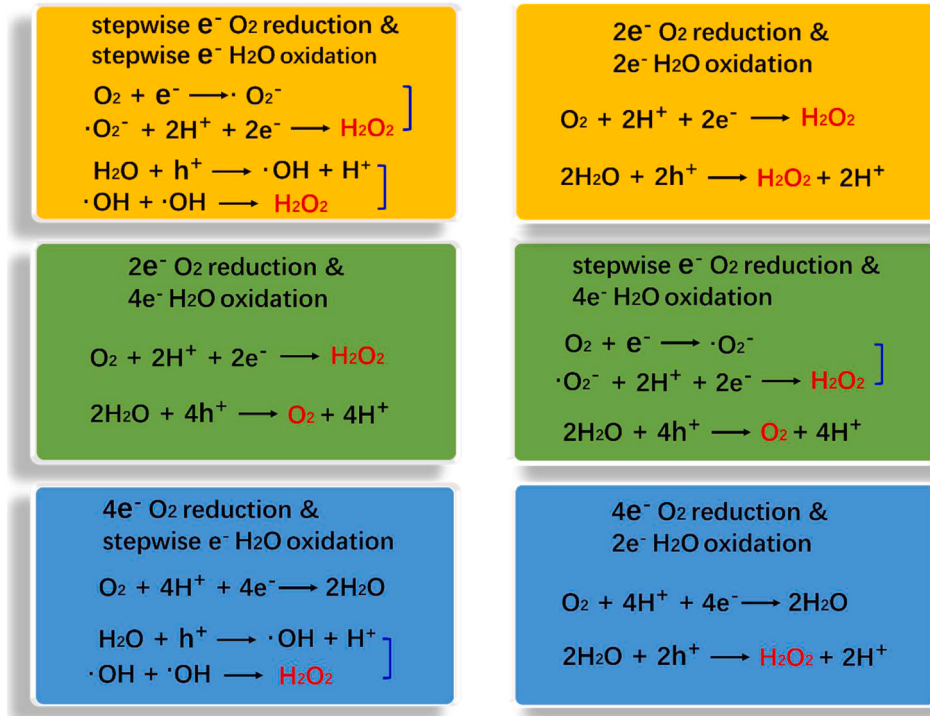


Fig. 3. Different combinations of oxygen reduction/water oxidation pathways.

criteria, the ideal band gap should be between 1.8 and 2.9 eV. In addition, the photocatalysts with high surface area are usually required to provide more active sites for O_2 adsorption/activation due to the low solubility of O_2 in aqueous media [28]. For a long time, the research has mainly focused on inorganic materials, such as TiO_2 , BiVO_4 , ZnS and CdS -based materials [29–33]. These semiconductors usually exhibit

narrow absorption range and low sunlight utilization rate (most notably in the ultraviolet region), furthermore, their limited variability is not conducive to the regulation of band structure and interface properties at the molecular level [30,31]. Therefore, the design and development of new photocatalytic materials is the key to achieving efficient, safe, green and sustainable H_2O_2 production.

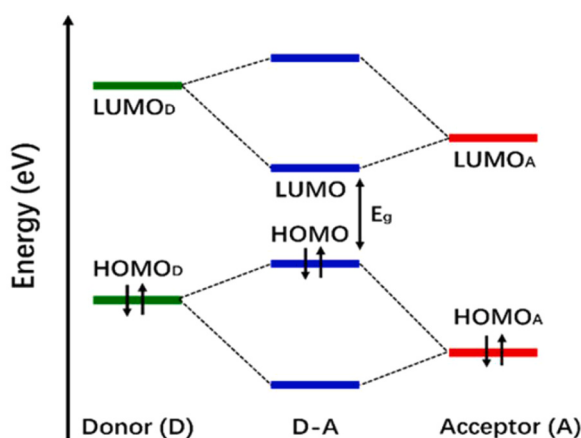


Fig. 4. Schematic illustration of optical band gap (E_g) in D-A system.

Metal-free organic polymers with semiconductor properties have attracted wide attention due to their unique electronic and optical properties [34–36]. They have great advantages in designability, adjustability and functionability [37–40]. The high specific surface area and porosity can expose more active sites, which promotes the contact between O_2/H_2O molecules and catalytic active centers, thereby improving the reaction rate [41,42]. In addition, the extended π -conjugated structure of organic polymers not only expands the light

absorption range to the visible region, but also facilitates photo-induced charges separation/transfer and inhibits recombination, maximizing the utilization of solar energy [43–45]. What's more, the modular construction of organic polymers provides a rich choice for the application of photocatalysis to regulate the catalyst composition, photoelectric properties and interface properties at the molecular level [46–48]. So that the CB/VB potential and band gap width can simultaneously meet the requirements of O_2 reduction and H_2O oxidation [49,50]. These distinctive features have attracted extensive attention and led to the rapid development of various metal-free-based photocatalysts with interesting structures and properties [51–55], but there is a pressing requirement to summarize and highlight the research status of photocatalytic H_2O_2 production by metal-free-based photocatalytic system.

In this review, a comprehensive summarization for organic polymers photocatalytic H_2O_2 production was presented (Fig. 1). The fundamental principles of photocatalytic H_2O_2 generation were first illustrated. Then, the elaborate design and synthesis of various metal-free-based photocatalysts, such as graphite carbon nitride ($g\text{-}C_3N_4$), covalent triazine frameworks (CTFs), covalent organic frameworks (COFs) and covalent organic polymers (COPs) with specific functional groups were discussed detailedly. The strategies for structure and property optimization of metal-free-based photocatalysts at molecular-level have been presented for the improvement of photocatalytic performance. The reaction mechanism has also been illustrated to promote further comprehension of photocatalytic H_2O_2 production. Furthermore, the structure-activity relationship was elaborated in detail to guide the construction of metal-free-based photocatalytic system with high-

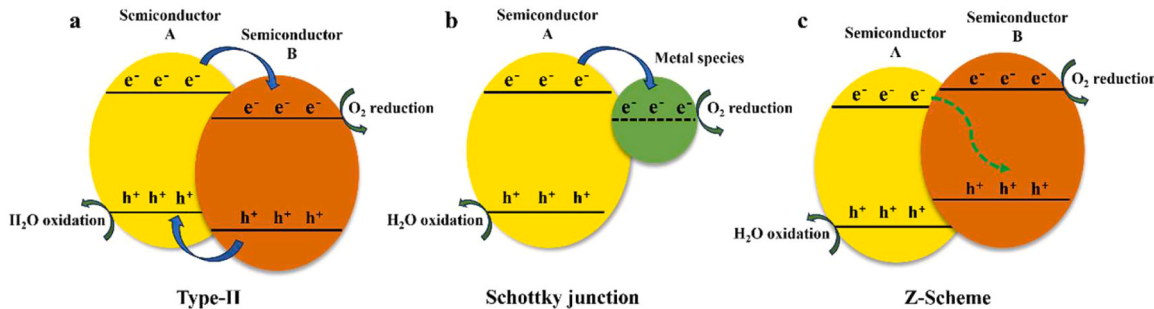


Fig. 5. The illustration of Type-II heterojunction (a), Schottky junction (b) and Z-scheme heterojunction (c).

Table 1
Summary of the reported photocatalytic H_2O_2 production by $g\text{-}C_3N_4$ based photocatalysts.

Photocatalyst	Sacrificial reagent	Irradiation conditions	H_2O_2 activity	AQE	Ref.
$g\text{-}C_3N_4$	Ethanol	$\lambda > 420$ nm	30 μmol (12 h)	12% (420 nm)	[83]
$g\text{-}C_3N_4/\text{PDI}$	H_2O	$\lambda > 420$ nm	50.6 μmol (12 h)	2.6% (420 nm)	[85]
$g\text{-}C_3N_4/\text{PDI}/\text{rGO}$	H_2O	$\lambda \geq 420$ nm	60. μmol (48 h)	6.1% (420 nm)	[119]
$g\text{-}C_3N_4/\text{BDI}$	H_2O	$\lambda > 420$ nm	41 μmol (48 h)	4.6% (420 nm)	[84]
$g\text{-}C_3N_4/\text{MTI}$	H_2O	$\lambda > 420$ nm	50 μmol (60 h)	6.2% (420 nm)	[86]
$g\text{-}C_3N_4/\text{AQ}$	2-Propanol	Simulated solar (100 mW cm^{-2})	361 mM h^{-1}	19.5% (420 nm)	[91]
Benzene/ $g\text{-}C_3N_4$	Ethanol	$\lambda > 420$ nm	290 μM (3 h)	N/A	[87]
K, P, O doped $g\text{-}C_3N_4$	Ethanol	$\lambda \geq 420$ nm	1.8 mM (7 h)	8.2% (420 nm)	[104]
KPF ₆ doped $g\text{-}C_3N_4$	Ethanol	$\lambda \geq 420$ nm	1 mM (3 h)	24.3% (420 nm)	[105]
K, S doped $g\text{-}C_3N_4$	Ethanol	$\lambda \geq 420$ nm	4.1 mM (3 h)	-	[106]
K doped $g\text{-}C_3N_4$	Isopropanol	$\lambda \geq 420$ nm	1800 μM (2.5 h)	20% (400 nm)	[107]
Cu doped $g\text{-}C_3N_4$	H_2O	400–800 nm	4.8 mM (6 h)	-	[108]
C, O co-doped $g\text{-}C_3N_4$	H_2O	$\lambda \geq 420$ nm	60.3 μmol (30 h)	7.23% (420 nm)	[109]
Au/ $g\text{-}C_3N_4$	2-propanol	UV/Vis	747 mmol (2 h)	3.63% (400 nm)	[110]
CoP/ $g\text{-}C_3N_4$	Ethanol	$\lambda > 420$ nm	70 mM h^{-1}	-	[111]
Co/ $g\text{-}C_3N_4$ -AQ	H_2O	Simulated solar (AM 1.5 G)	62 $\mu\text{M h}^{-1}$	-	[93]
In(III)/ $g\text{-}C_3N_4$	Ethanol	$\lambda > 420$ nm	7.5 mg L^{-1}	-	[112]
$g\text{-}C_3N_4$ with carbon vacancies	H_2O	$\lambda > 420$ nm	95 μM (1 h)	-	[97]
$g\text{-}C_3N_4$ with nitrogen vacancies	2-Propanol	$\lambda > 420$ nm	12.1 μmol (2.5 h)	9.2% (420 nm)	[94]
Mesoporous $g\text{-}C_3N_4$	Ethanol	$\lambda > 420$ nm	90 μmol (24 h)	-	[70]
Hierarchical $g\text{-}C_3N_4$	Ethanol	Simulated solar	3249 μM (3 h)	0.088% (365 nm)	[113]
$g\text{-}C_3N_4$ aerosol gel	H_2O	$\lambda > 420$ nm	36 μmol (25 h)	-	[114]

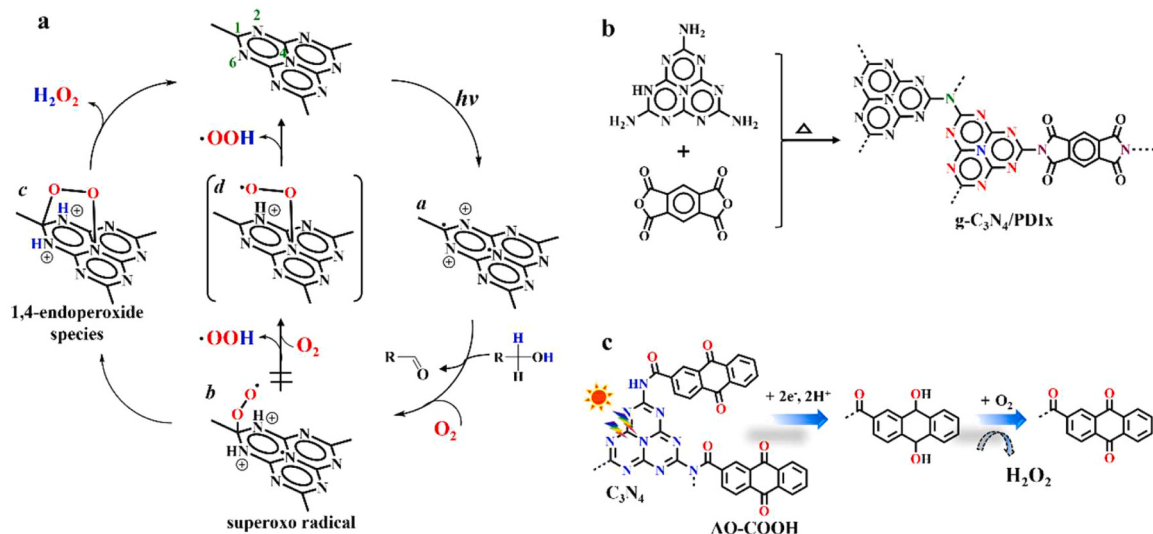


Fig. 6. The proposed mechanism of selective photocatalytic H₂O₂ formation by pristine g-C₃N₄ (a); the synthesis of g-C₃N₄/PDI (b); the photocatalytic H₂O₂ production process of AQ decorated g-C₃N₄ under visible light irradiation (c).

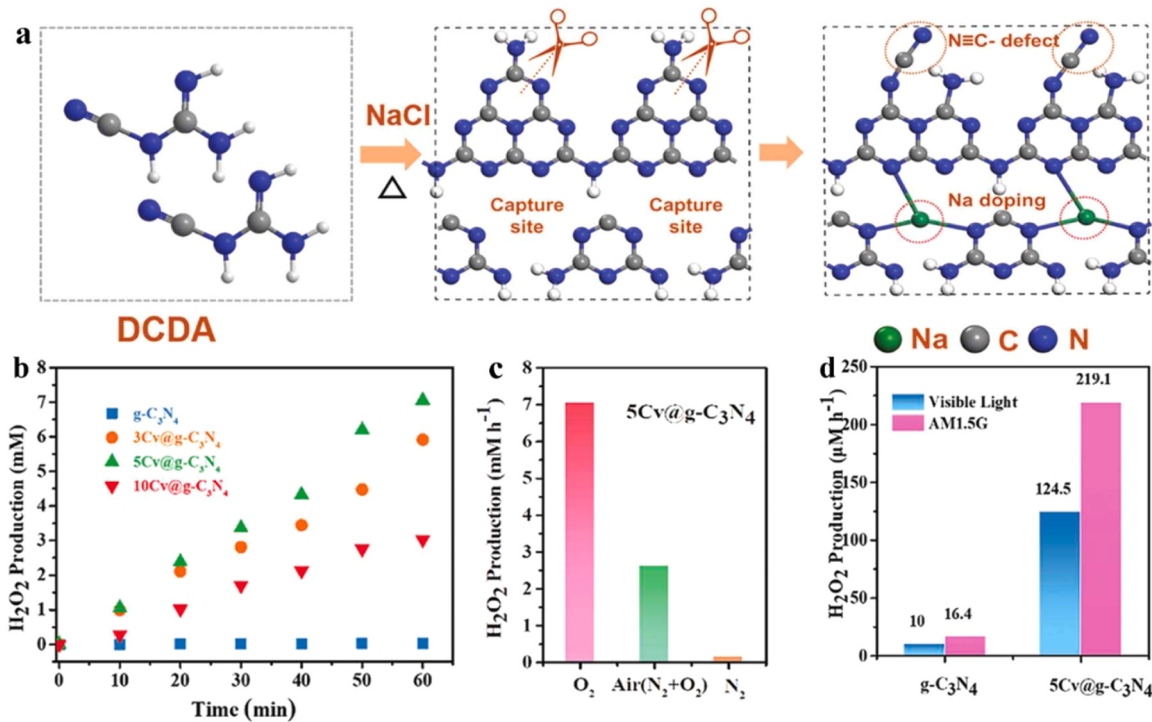


Fig. 7. The synthesis schematic of cyano-rich graphitic carbon nitride (Cv@g-C₃N₄) induced during ionothermal process (a); the kinetic profile of H₂O₂ production of Cv@g-C₃N₄ and g-C₃N₄ (b); the photocatalytic H₂O₂ production of 5Cv@g-C₃N₄ under various atmosphere (c); the photocatalytic H₂O₂ production of 5Cv@g-C₃N₄ and g-C₃N₄ in pure water (d). Copyright 2021 Wiley-VCH.

Adapted with permission from ref 99.

performance. In general, this review provides a new insight of specific photocatalysis for solar to chemical energy conversion.

2. Principles of the photocatalytic H₂O₂ production

2.1. Pathway of photocatalytic H₂O₂ production

In theory, the photocatalytic production of H₂O₂ can be realized through both two-electron oxygen reduction path and two-electron water oxidation path [56–60]. However, either two-electron oxygen

reduction or water oxidation path has the corresponding one- and four-electron paths to compete with them [59]. Compared with the four-electron oxygen reduction/water oxidation path, the one-electron or two-electron path is more dynamic efficient despite they need to overcome a higher redox potential ($-0.33\text{ V}/2.73\text{ V}$ or $0.68\text{ V}/1.76\text{ V}$ vs $1.23\text{ V}/1.23\text{ V}$) in thermodynamically (Fig. 2) [61,62]. Therefore, as long as the redox potential of photocatalytic materials can meet the requirements for thermodynamic oxygen reduction and water oxidation reactions. That is to say, the CB and VB of photocatalytic materials can cross the potential range of single-electron oxygen reduction/water

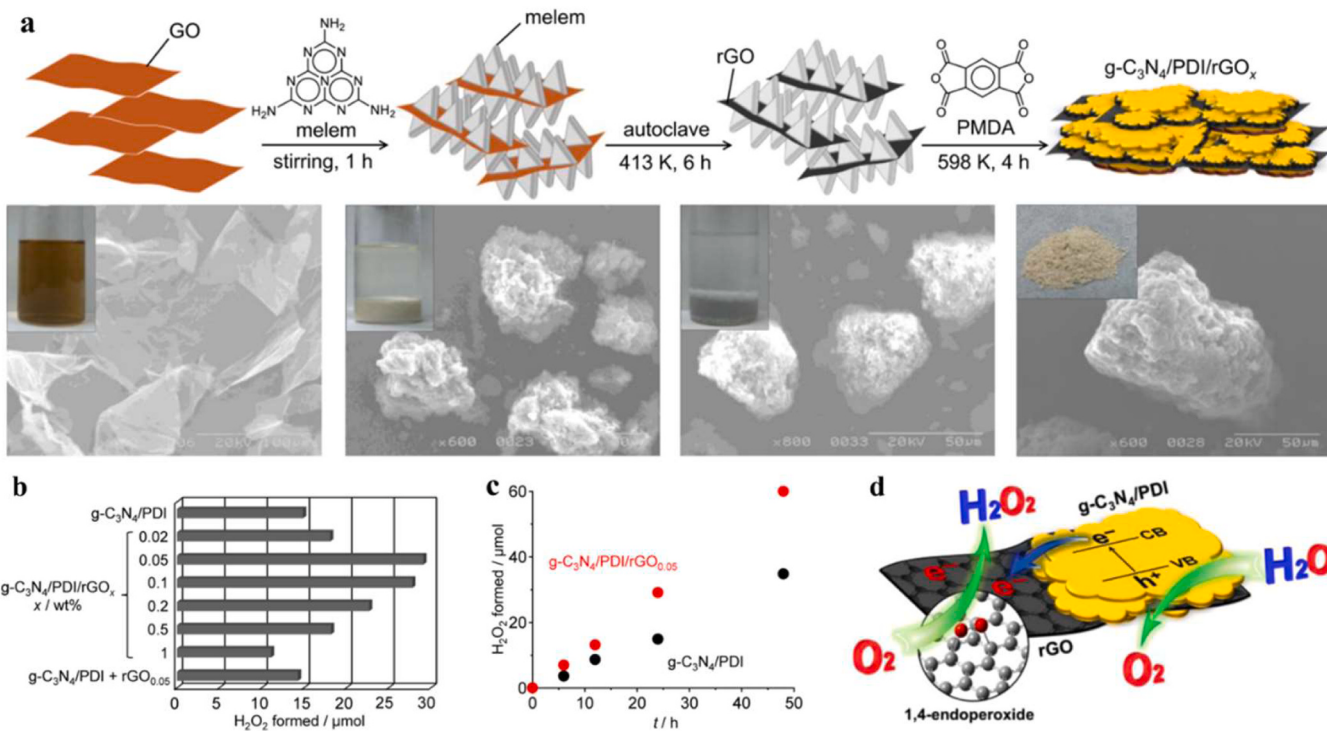


Fig. 8. The synthesis illustration of g-C₃N₄/PDI/rGO_{0.05}, photographs and scanning electron microscopy (SEM) images (a); the performance of photocatalytic H₂O₂ production for the respective catalysts (b); the time-dependent hotocatalytic H₂O₂ production for g-C₃N₄/PDI/rGO_{0.05} and g-C₃N₄/PDI (c); the schematic illustration for proposed mechanism of photocatalytic H₂O₂ production in the presence of g-C₃N₄/PDI/rGO (d). Copyright 2016 American Chemical Society.

Adapted with permission from ref 119.

Table 2
Summary of the reported photocatalytic H₂O₂ production by COFs based photocatalysts.

Photocatalyst	Sacrificial reagent	Irradiation conditions	H ₂ O ₂ activity	AQE	Ref.
TAPD-(Me) ₂ COF	H ₂ O:EtOH (9:1)	420–700 nm	97 μmol g ⁻¹ h ⁻¹	-	[136]
TAPD-(OMe) ₂ COF	H ₂ O:EtOH (9:1)	420–700 nm	91 μmol g ⁻¹ h ⁻¹	-	[136]
SonoCOF-F ₂	H ₂ O	≥ 420 nm	8.20 μmol g ⁻¹ h ⁻¹	4.8% (420 nm)	[135]
EBA-COF	H ₂ O: BA (9:1)	= 420 nm	2550 μmol g ⁻¹ h ⁻¹	-	[137]
BTEA-COF	H ₂ O:EtOH (9:1)	= 420 nm	780 μmol g ⁻¹ h ⁻¹	-	[137]
COF-TfyBpy	H ₂ O	420–700 nm	1042 μmol g ⁻¹ h ⁻¹	-	[138]
CoPC-BTMCOF	H ₂ O:EtOH (9:1)	≥ 420 nm	2096 μmol g ⁻¹ h ⁻¹	7.2% (420 nm)	[128]
CoPC-DABCDF	H ₂ O:EtOH (9:1)	≥ 420 nm	1815 μmol g ⁻¹ h ⁻¹	5.2% (420 nm)	[128]
HEP-TAPT-COF	H ₂ O	> 420 nm	1750 μmol g ⁻¹ h ⁻¹	15.35% (420 nm)	[142]
HEP-TAPB-COF	H ₂ O	> 420 nm	990 μmol g ⁻¹ h ⁻¹	9.98% (420 nm)	[142]
COF TTA-TTTA	H ₂ O	~ 420 nm	36.10 μmol h ⁻¹	-	[143]
COF TTA-TA	H ₂ O	~ 420 nm	33.90 μmol h ⁻¹	-	[143]
N ₀ -COF	H ₂ O	= 495 nm	15.70 μmol h ⁻¹	-	[140]
DMCR-1 (COF)	H ₂ O:IPA (10:1)	420–700 nm	2264 μmol g ⁻¹ h ⁻¹ 1617 μmol g ⁻¹ h ⁻¹	8.8% (420 nm) 7.2% (420 nm)	[123]
Imine-1 (COF)			2588 μmol g ⁻¹ h ⁻¹	10.2% (420 nm)	
DMCR-1NH (COF)					
TF50-COF	EtOH	> 400 nm	1739 μmol g ⁻¹ h ⁻¹	5.1% (400 nm)	[139]
TTF-BT-COF	H ₂ O	≥ 420 nm	276,000 μM g ⁻¹ h ⁻¹	11.19% (420 nm)	[144]
Py-Da-COF	H ₂ O:EtOH (9:1)	420–700 nm	461 μmol g ⁻¹ h ⁻¹	2.4% (420 nm)	[133]
COF-TAPB-BPDA	H ₂ O:BA (4:1)	> 420 nm	1240 μmol g ⁻¹ h ⁻¹	-	[134]
TDB-COF	H ₂ O	Simulated solar (AM 1.5 G)	723.5 μmol g ⁻¹ h ⁻¹	1.4% (400 nm)	[125]
4PE-N-S COF	H ₂ O	420–700 nm	1574 μmol g ⁻¹ h ⁻¹	-	[132]
TAPB-PDA-OH	H ₂ O:EtOH (9:1)	> 420 nm	2117.6 μmol g ⁻¹ h ⁻¹	2.99% (420 nm)	[131]
TpAQ-COF-12	H ₂ O	> 420 nm	420 μmol g ⁻¹ h ⁻¹	7.4% (420 nm)	[127]
FS-COFs	H ₂ O	> 420 nm	3904.2 μmol g ⁻¹ h ⁻¹	6.21% (420 nm)	[126]
COF-NUST-16	H ₂ O:EtOH (9:1)	≥ 420 nm	1081 μmol g ⁻¹ h ⁻¹	-	[130]

oxidation, the single-electron path will be preferentially carried out. In addition, the O₂[·] and ·OH generated from single-electron oxygen reduction/water oxidation path could further convert to H₂O₂ via the stepwise single-electron path (O₂ + e⁻ → O₂[·] + e⁻ → H₂O₂ and H₂O + e⁻ → ·OH + e⁻ → H₂O₂), which is more advantageous than the four-electron path in promoting photocatalytic H₂O₂ production [56]. Based on the above

analysis, to achieve the goal of efficient H₂O₂ production, the corresponding photocatalytic materials should not only have appropriate band structure, but also be able to effectively inhibit the competition of four-electron path and improve the selectivity of H₂O₂ production path. In recent years, the focus of relevant researchers has gradually shifted from how to improve the efficiency of reduction paths such as step by

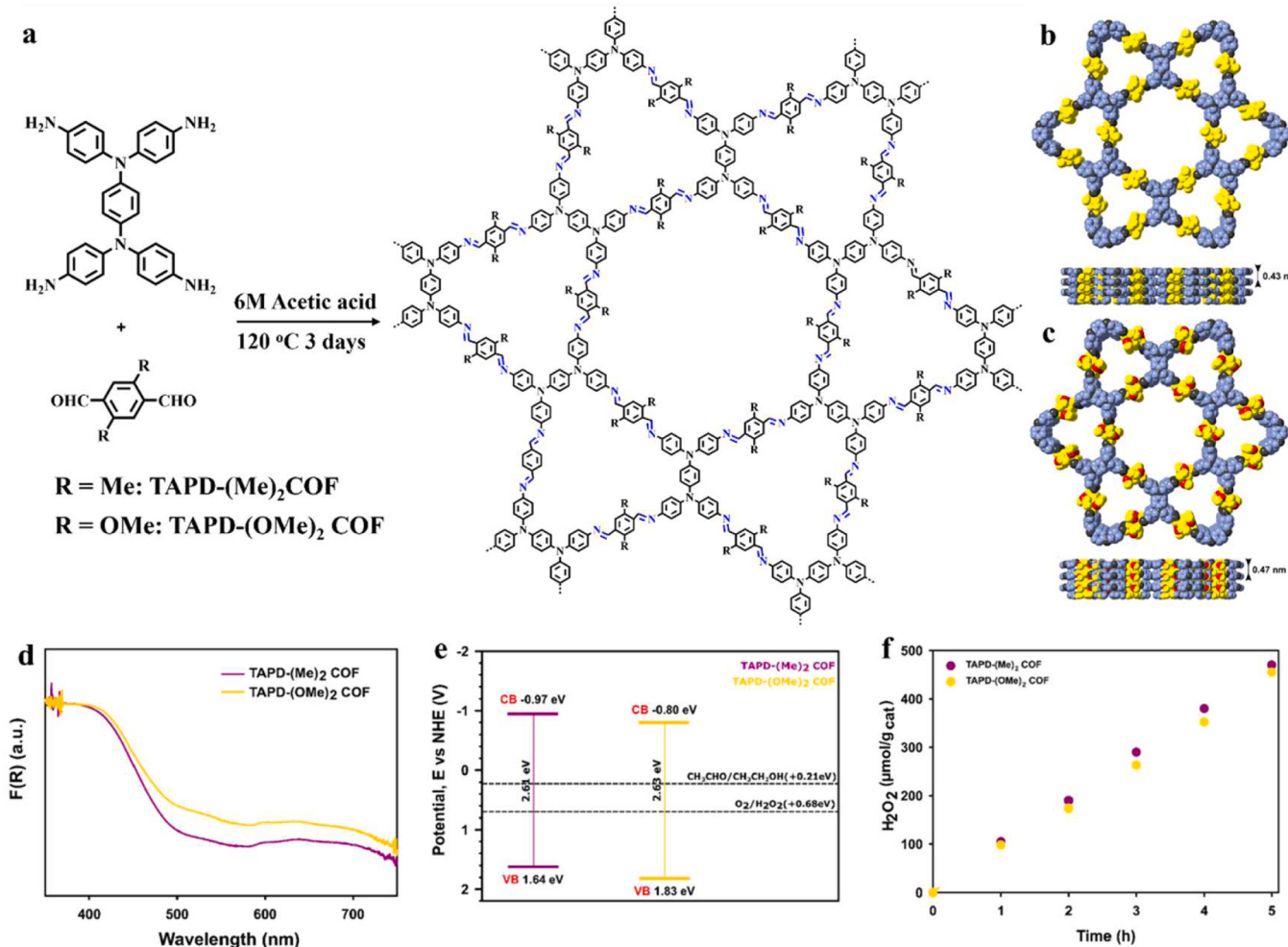


Fig. 9. The schematic illustration of TAPD-(Me)₂ and TAPD-(OMe)₂ COFs (a); the top and side views of TAPD-(Me)₂ (b) and TAPD-(OMe)₂ COFs (c); the solid state UV-vis spectra (d), band potential (e) and time-dependent H₂O₂ production (f) of TAPD-(Me)₂ and TAPD-(OMe)₂ COFs. Copyright 2020 American Chemical Society. Adapted with permission from ref 136.

step single electron or step by step two-electron oxygen reduction to produce H₂O₂, to account the single electron water oxidation production-OH to replace the traditional four-electron O₂ production path, so as to realize the redox dual-path for H₂O₂ production [63–65]. It should be mentioned that the amount of H₂O₂ produced by photocatalysis technology is still very low to satisfy the requirements of practical applications such as water treatment (concentration≈30 mmol·L⁻¹), although some research progress has been made, such as nanomole production and solar energy conversion efficiency higher than that of green plant photosynthesis (0.1%) [66]. Therefore, how to further improve the efficiency of photocatalytic H₂O₂ production is still a pressing challenge that must be overcome before the industrialization of this technology.

2.2. The influence factors for photocatalytic H₂O₂ production

To further improve the efficiency of photocatalytic H₂O₂ production, the specific steps involved in the photocatalytic H₂O₂ production process should be fully understood and the limiting factors of each step should be mastered. In general, the whole photocatalytic H₂O₂ production process can be divided into three steps: light absorption, charge separation and surface reaction, and the final H₂O₂ generation rate is determined by the above steps [27]. Improving the efficiency of each step will help promote the whole efficiency of H₂O₂ production.

The narrow absorption range, low utilization rate of light energy and

easy recombination of photogenerated carriers are common problems of photocatalytic materials [67]. The common approaches to solve the above problems are as follows: for example, the construction of heterojunction [68], doping elements [69], the introduction of defects etc [70]. The absorption range of photocatalytic materials can be extended to visible region through reasonably designing composition and structure. Furthermore, the separation and transfer of photo-generated charges could be effectively promoted by the construction of internal electric field and intermediate band gap [71]. Notably, for photocatalytic H₂O₂ production reaction, if the incorporated components, elements or defects can play the role of active sites in the oxygen reduction/water oxidation process, the above method also has the ability to improve the efficiency of surface reaction, so it has extensive research value.

On the other hand, for photocatalytic H₂O₂ production reaction, the efficiency of oxygen reduction and water oxidation process is a more direct factor restricting the whole H₂O₂ production efficiency [72,73]. Therefore, how to restrain the competition of four-electron oxygen reduction/water oxidation path, so that improve the selectivity of one-electron and two-electron paths is undoubtedly the key to solving the above problems (Fig. 3). Compared with the water oxidation path, there are more studies on the oxygen reduction path for H₂O₂ production, and its mechanism is more definite. The efficient conversion from O₂ to H₂O₂ can be achieved by introducing active groups or noble metal co-catalyst modification [74,75]. However, the high kinetic barrier of

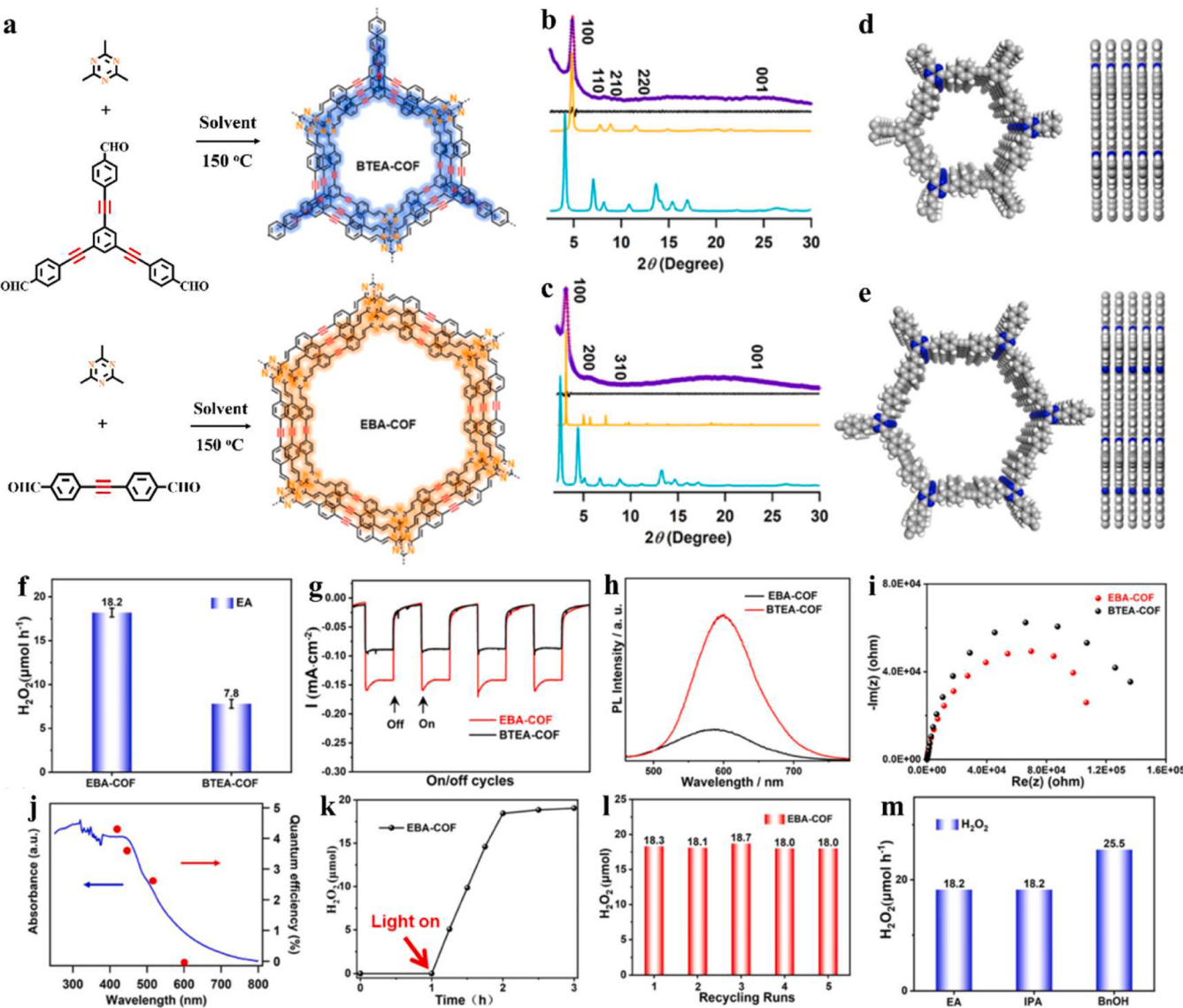


Fig. 10. The schematic illustration of BTEA-COF and EBA-COF (a); PXRD patterns of BTEA-COF (b) and EBA-COF (c); Top view and side view of the AA packing model of BTEA-COF (d) and EBA-COF (e); H_2O_2 generation rates (f), transient photocurrents (g), photoluminescence emission spectra (h), electrochemical impedance spectra (i) of BTEA-COF and EBA-COF; wavelength-dependent AQE (j), time-dependent H_2O_2 generation (k), photocatalytic H_2O_2 generation cycles (l), H_2O_2 generation in different sacrificial reagents (m) for EBA-COF. Copyright 2022 American Chemical Society. Adapted with permission from ref 137.

the four-electron water oxidation path is still the main factor restricting the water oxidation reaction and the overall efficiency of H_2O_2 production [76]. In addition, the generated H_2O_2 cannot be separated from the catalyst surface in time, which will not only be consumed by photo-induced holes, but also cause the catalyst poisoning and lead to reduced activity [77]. Therefore, how to improve the efficiency of water oxidation reaction and prevent the generated H_2O_2 from being decomposed are also the direction of researchers' efforts.

3. The design and synthesis of metal-free-based photocatalysts

Compared with traditional inorganic photocatalysts, organic polymers as photocatalysts have the advantages of simple synthesis methods, wide monomer sources, catalysts designability and sensitivity to visible light [34,46]. Based on the abundant preparation methods of organic polymers, the chemical and physical properties such as electronic structure, surface catalytic site and structural stability can be highly regulated by adjusting the structure of organic polymers [56]. In

addition, the pore shape and size of organic polymers can be finely controlled by topology and monomer length regulation, and their structures are regular, ordered and highly crystalline [55], which can promote the effective separation and migration of photogenerated charges, and has a wide range of application prospects and research value in the field of photocatalysis.

3.1. Intrinsic structure design

The efficient separation and rapid migration of photo-generated carriers is the key to improving the efficiency of solar energy conversion. The construction of donor-acceptor (D-A) system with alternating electron donor (D) and acceptor (A) can effectively reduce the intramolecular exciton binding energy and improve the photogenerated charge separation efficiency based on previous theoretical studies and experiments (Fig. 4) [52,53]. The organic polymers semiconductor catalysts with different band structures and bandgap widths can be obtained by selecting appropriate electron donor and acceptor building

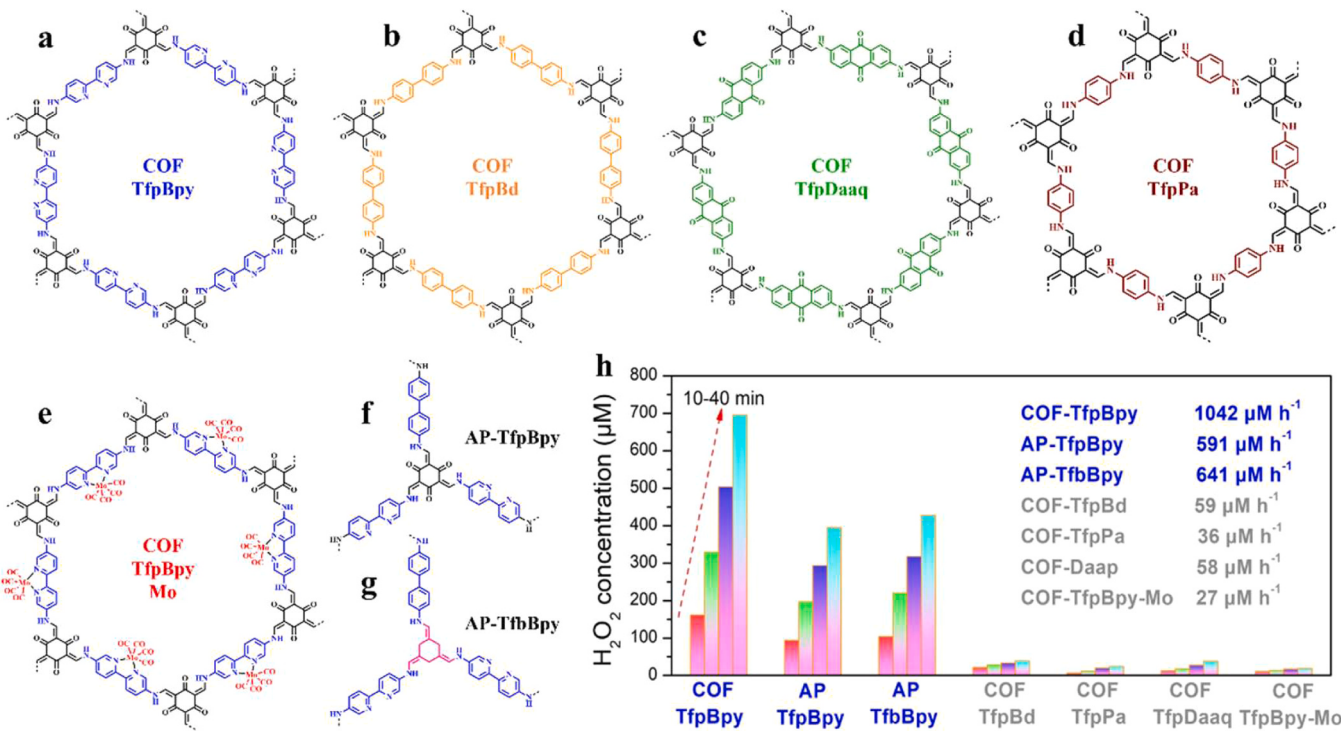


Fig. 11. The chemical structures of COF-TfpBpy (a), COF-TfpBd (b), COF-TfpDaaq (c), COF-TfpPa (d), COF-TfpBpy-Mo (e), AP-TfpBpy (f) and AP-TfpBd (g); the photocatalytic H_2O_2 generation rates of different COFs and amorphous polymer (h). Copyright 2022 Wiley-VCH. Adapted with permission from ref 138.

blocks [52]. So as to meet the requirements of CB/VB potential and band gap width for O_2 reduction and H_2O oxidation at the same time. Furthermore, the strong electron push and pull effect between electron donor and acceptor can extend the absorption range of DA-photocatalysts to the visible region, accelerate photogenerated electrons and holes separation, improve carriers separation efficiency, and inhibit their recombination. In addition, the large specific surface area can provide more active sites for O_2 adsorption, increase the local O_2 concentration on the catalyst surface, and capture photogenerated electrons. The designability can introduce guiding groups on the catalyst surface, promote the aggregation of H_2O molecules on the catalyst surface through hydrogen bond interaction, and accelerate the reaction.

3.2. Heterojunction structure design

The single photocatalyst usually faces two problems: 1) the narrow band gap is required for wide sunlight absorption, but which inevitably suppresses the redox capacity of photocatalyst; 2) the rapid recombination of photogenerated electron-hole pairs due to strong coulomb gravity [50,78]. Therefore, it is necessary to modify the photocatalyst to reduce the recombination rate of photogenerated carriers and broaden the light absorption. The heterojunction of two kinds of semiconductors with interleaving band structure can not only broaden the absorption range of light, but also adjust the band gap width and redox capacity [32,42]. In order to promote the separation and transfer of photo-induced carriers, the construction of heterojunction is an effective method to solve the problem of band gap incompatibility and improve the performance of photocatalysis. Among heterojunctions, the Type-II heterojunction, Schottky junction and Z-scheme are most reported due to their high efficiency in charge space separation and interfacial transfer (Fig. 5) [50,54,68]. In the Type-II heterojunction, semiconductors A and B have a unique band interleaving structure, and the VB and CB of semiconductor A are higher than those of semiconductor B, respectively (Fig. 5a) [50]. Schottky junction is a special form of heterojunction, which is composed of semiconductor and metal species, and

this structure facilitates the formation of space charge separation regions (Fig. 5b) [54]. In Z-scheme heterojunction system, the two semiconductors are not in direct contact, and the carrier in the system is transferred through ions in solution (Fig. 5c) [68].

4. Photocatalytic H_2O_2 production by metal-free photocatalysts

4.1. Photocatalytic H_2O_2 production by graphite carbon nitride ($\text{g-C}_3\text{N}_4$)

Graphite carbon nitride ($\text{g-C}_3\text{N}_4$) is a typical polymer semiconductor, the C and N atoms in $\text{g-C}_3\text{N}_4$ are hybridized with sp^2 to form a highly delocalized π -conjugated system [79]. It can be prepared by facile heat treatment of nitrogen-rich precursors, such as melamine, cyanamide, thiourea, urea and dicyandiamide etc. Since Wang et al. discovered that the $\text{g-C}_3\text{N}_4$ could be used as metal-free photocatalyst for H_2 production in 2009 [80], which has attracted extensive attention in the field of photocatalysis due to its advantages such as simple preparation, low cost, stable structure and suitable energy band structure, showing a huge potential application prospect [25].

The band gap of $\text{g-C}_3\text{N}_4$ is about 2.7 eV, and it can absorb ultraviolet and visible light with wavelength less than 460 nm [81]. The conduction band is -1.3 V vs. NHE (versus Normal Hydrogen Electrode), which is more negative than the potential required by reduction of O_2 to produce H_2O_2 ($E(\text{O}_2/\text{H}_2\text{O}_2) = 0.68$ V vs. NHE) [81,82]. And its valence band is located at $+1.4$ V vs. NHE, which theoretically meets the potential energy requirement ($E(\text{H}_2\text{O}/\text{O}_2) = 1.23$ V vs. NHE) for O_2 formation from H_2O oxidation reaction [81,82]. Therefore, when it is applied to the photocatalytic H_2O_2 production reaction, the mechanism can be described by two half reactions [27]: (1) Photogenerated holes oxidize H_2O to O_2 through the four-electron path; (2) Photogenerated electrons reduce O_2 to H_2O_2 through the two-electron path. The total reaction of photocatalytic H_2O_2 production by $\text{g-C}_3\text{N}_4$ can be described as $\text{H}_2\text{O} + 1/2 \text{O}_2 \rightarrow \text{H}_2\text{O}_2$. Table 1 summarizes the recently reported photocatalytic H_2O_2 production by $\text{g-C}_3\text{N}_4$ based materials. In 2014, Shiraishi et al. first reported the $\text{g-C}_3\text{N}_4$ as catalyst for selective photocatalytic

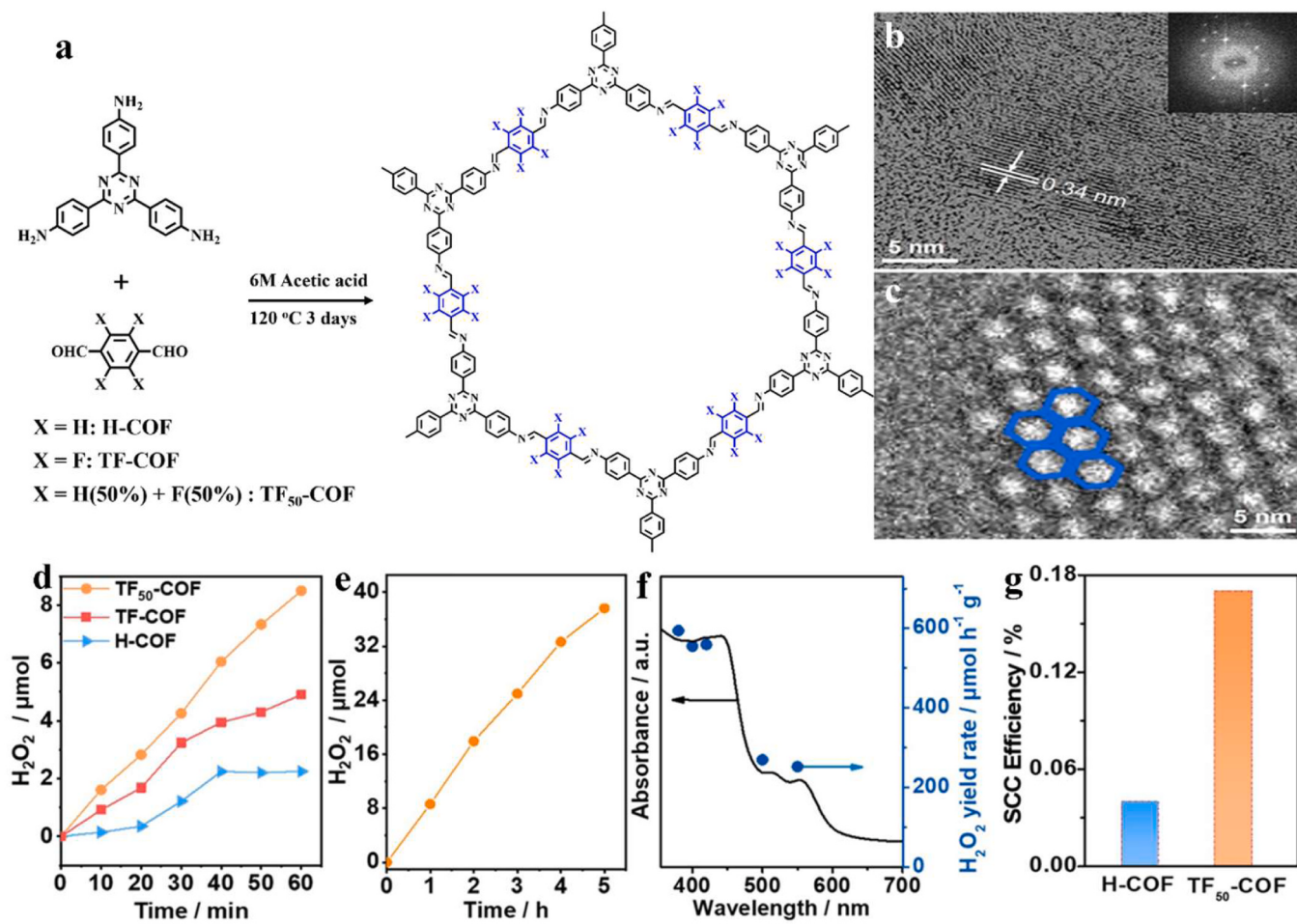


Fig. 12. The schematic illustration of H-COF, TF-COF and TF₅₀-COF (a); TEM images of TF₅₀-COF (b, c); time-dependent H₂O₂ generation of H-COF, TF-COF and TF₅₀-COF (d); photocatalytic H₂O₂ generation rate and wavelength dependent H₂O₂ yields of TF₅₀-COF (e, f); the SCC efficiencies of H-COF and TF₅₀-COF (g).

Copyright 2022 Wiley-VCH.

Adapted with permission from ref 139.

H₂O₂ production from 2e⁻ O₂ reduction under the irradiation of sunlight ($\lambda > 400$ nm) [83]. The high selective 2e⁻ O₂ reduction pathway for photocatalytic H₂O₂ production can be attributed to the efficient 1, 4-endoperoxide species formation on g-C₃N₄ surface by stepwise one-electron process (Fig. 6a). The rapidly generated endoperoxide suppressed ·OOH radical formation, which was conducive to selective two-electron O₂ reduction reaction. However, ethanol was required as electron sacrificial agent to promote this reaction because the H₂O oxidation capacity of pure g-C₃N₄ was not satisfactory. To achieve photocatalytic H₂O₂ production from H₂O and O₂ without additional alcohol as sacrificial agent, the photo-induced h⁺ must be thermodynamically able to oxidize H₂O. The most obvious methods are to regulate photocatalyst's VB potential by incorporating functional groups in the framework of g-C₃N₄ [84–90]. Shiraishi et al. reported a simple modification of g-C₃N₄ to tune the redox potential by incorporating various aromatic diimides, like biphenyl diimide(BDI), pyromellitic diimide (PDI), and mellitic triimide (MTI) (Fig. 6b) [84–86]. The introduced electron-withdrawing groups with high electron affinity could positively shifted VB levels of pristine g-C₃N₄ photocatalysts, which facilitated H₂O oxidation process, thus promoting the photocatalytic H₂O₂ production. Furthermore, the photo-induced e⁻ and h⁺ are located on the melem and BDI moieties of g-C₃N₄/BDI catalyst, respectively, which is conducive to suppressing the recombination of photo-generated charges [84]. In addition, the g-C₃N₄ doped with MTI functional group by thermal condensation created a condensed melem layer, which promoted efficient intra- and interlayer photo-generated charges migration in the

g-C₃N₄/MTI and exhibited a higher electrical conductivity than that of g-C₃N₄/PDI [85,86]. The g-C₃N₄/MTI exhibited efficient photocatalytic H₂O₂ production with millimolar levels via photo-induced h⁺ oxidizing H₂O and photo-induced e⁻ reducing O₂ under visible light ($\lambda > 420$ nm) irradiation [86]. In general, with the incorporation of various aromatic diimide groups into the network of g-C₃N₄, the prepared composite g-C₃N₄-based photocatalysts exhibited higher activity and selectivity for photocatalytic H₂O₂ production from H₂O and O₂ under visible light irradiation.

The anthraquinone (AQ) molecule possesses satisfactory selectivity in H₂O₂ production reaction and has been widely used for industrial H₂O₂ production [27]. Inspired by this point, Kim et al. introduced the AQ functional group into g-C₃N₄ network by directly covalent bonding of pristine g-C₃N₄ and anthraquinone-2-carboxylic acid (AQ-COOH) (Fig. 6c) [91]. As a redox center, the incorporated AQ moieties significantly suppressed charges recombination and ultimately promoted quantum yield of g-C₃N₄ [91–93]. Furthermore, the AQ redox center effectively optimized electrons migration by initiating the hydrogenation reaction of AQ to form anthrahydroquinone (AQH₂), which subsequently drove O₂ reduction to H₂O₂ via dehydrogenation reaction of AQH₂ and regenerated to AQ. The rational design with specific AQ redox center can result in selective photocatalytic H₂O₂ formation. Moreover, the AQ moieties on g-C₃N₄ network could suppress decomposition of H₂O₂ generated by photocatalysis. The AQ reinforced g-C₃N₄ (10% wt) could achieve an optimal photocatalytic H₂O₂ production rate of 361 μmol g⁻¹ h⁻¹ under the irradiation of simulated solar.

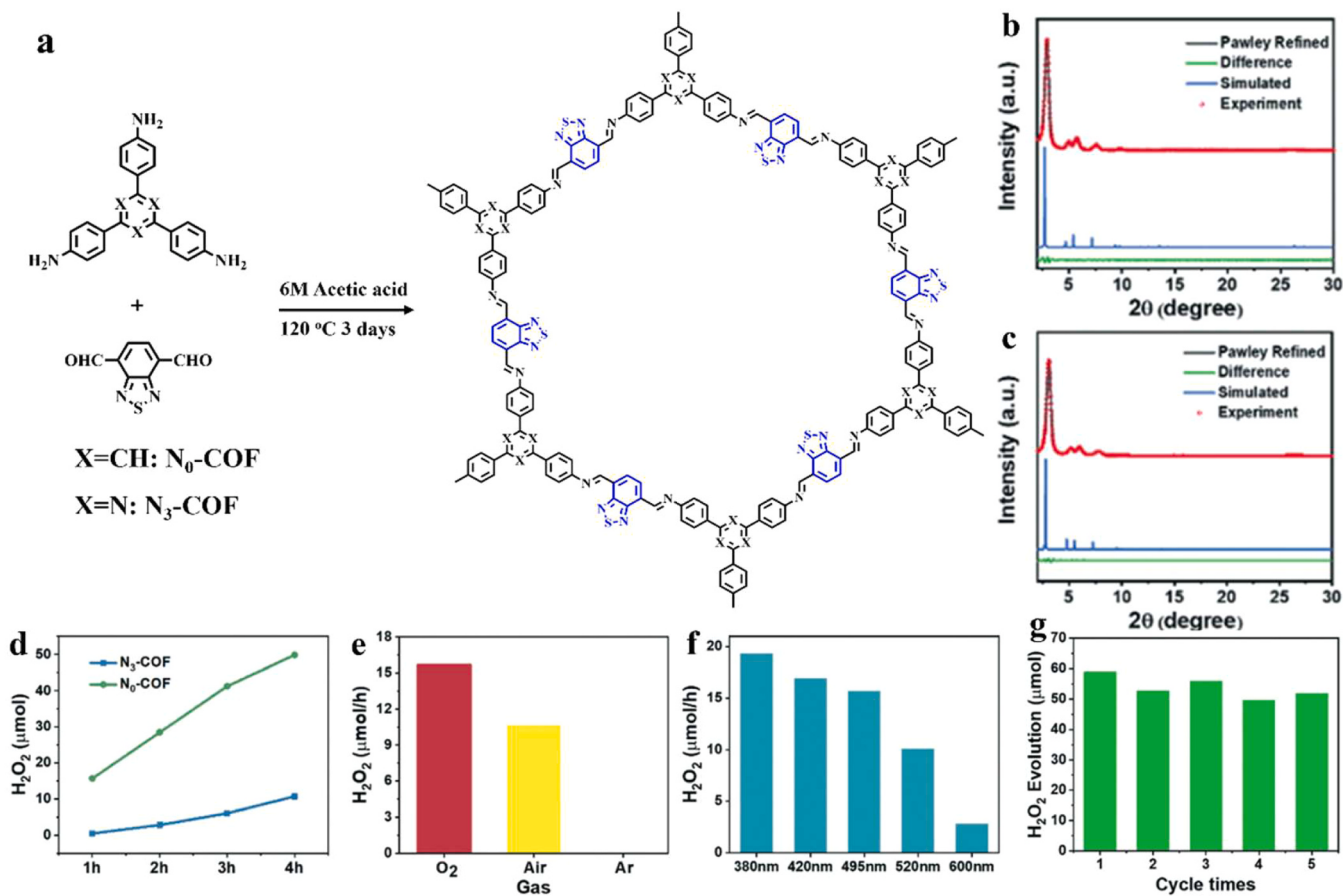


Fig. 13. The schematic illustration for Nx-COFs (a); the PXRD patterns of N₀-COF (b) and N₃-COF (c); time-dependent H₂O₂ generation of N₀-COF and N₃-COF (d); reaction activities under different atmospheres (e) and different wavelengths (f) of N₀-COF; The cycles of N₀-COF in photocatalytic H₂O₂ evolution (g). Copyright 2022 Royal Society of Chemistry.

Adapted with permission from ref 140.

Introducing defects into g-C₃N₄ is also an effective way to improve its photocatalytic performance [94–97]. The defects modification will form defect levels between VB and CB, which could expand the range of light absorption and promote the separation of internal photogenerated carriers. On the other hand, the introduced defects can also act as the activation site of the reactants to improve the efficiency of the redox reaction. Quan et al. reported a facile method to promote efficiency of photocatalytic H₂O₂ production by incorporating alkali metals and making N vacancies on g-C₃N₄ network [98]. The incorporation of alkali metals with N vacancies could broaden light absorption region, decrease band gap, and significantly suppress photo-induced charges recombination. The cooperative interaction of alkali metal doping and N defect greatly promoted the performance of photocatalytic H₂O₂ production with a rate of 10.2 mmol g⁻¹ h⁻¹, which was 89.5 times higher than that of pristine g-C₃N₄. This work provides a new insight into the cooperative interaction of alkali metal doping and N defect for simultaneously regulating light harvesting and charges separation, then promoting the development of photocatalysts for efficient H₂O₂ production.

The above strategy optimizes photocatalytic activity, but the simultaneous regulations of activity and selectivity by making defects on g-C₃N₄ network is ignored. Chen et al. successfully synthesized g-C₃N₄ with Na doping and cyano group (-C≡N) defects (Cv@g-C₃N₄) by facile NaCl-assisted calcination approach (Fig. 7a), which could simultaneously improve activity and selectivity of photocatalytic H₂O₂ production [99]. The cyano groups in Cv@g-C₃N₄ not only tuned the band gap to boost light harvesting, but also served as O₂ active sites, in which the local charge polarization could accelerate O₂ adsorption and subsequent protonation. Then, the activated O₂ could be reduced to

superoxide radicals with the assistance of Na⁺, which are the key intermediates for 2e⁻ photocatalytic H₂O₂ production. The Cv@g-C₃N₄ showed superior H₂O₂ production activity of 7.01 mM h⁻¹ under visible light irradiation ($\lambda \geq 420$ nm) and high 2e⁻ selectivity (93%), which were much higher than that of pristine g-C₃N₄ (Fig. 7b). The control experiment indicated that the highest H₂O₂ generation rate was achieved under O₂-atmosphere, which decreased under air-atmosphere, and almost completely suppressed under N₂ atmosphere (Fig. 7c), demonstrating that H₂O₂ was generated via 2e⁻ O₂ reduction not 2e⁻ H₂O oxidation. It should be mentioned that the Cv@g-C₃N₄ is also efficient for H₂O₂ generation in pure water (Fig. 7d). Generally, this work provides a new method to simultaneously regulate activity and selectivity for efficient photocatalytic H₂O₂ production. Heteroatom doped g-C₃N₄ has been frequently employed to improve photocatalytic performance [100,101], but the structure-activity relationship understanding remains a challenge. Choi et al. revealed that the local charge polarization could enhance the adsorption of O₂ on photocatalysts and the synergistic effects of K bridging and S substitution facilitates H₂O₂ production by both spectroscopic studies and theoretical calculations, which provides a better understanding of the photocatalytic mechanism on how heteroatom dopants synergically work to make ORR (oxygen reduction reaction) effective and selective toward H₂O₂ production [100].

The construction of heterojunction and/or hybridization is an effective approach to solve the problems of narrow absorption range and prone to recombination of photo-generated charges in g-C₃N₄ based photocatalytic system [102–114]. The selectivity of heterojunction for oxygen reduction to H₂O₂ and the efficiency of driving water oxidation reaction should also be considered when applied to the photocatalytic

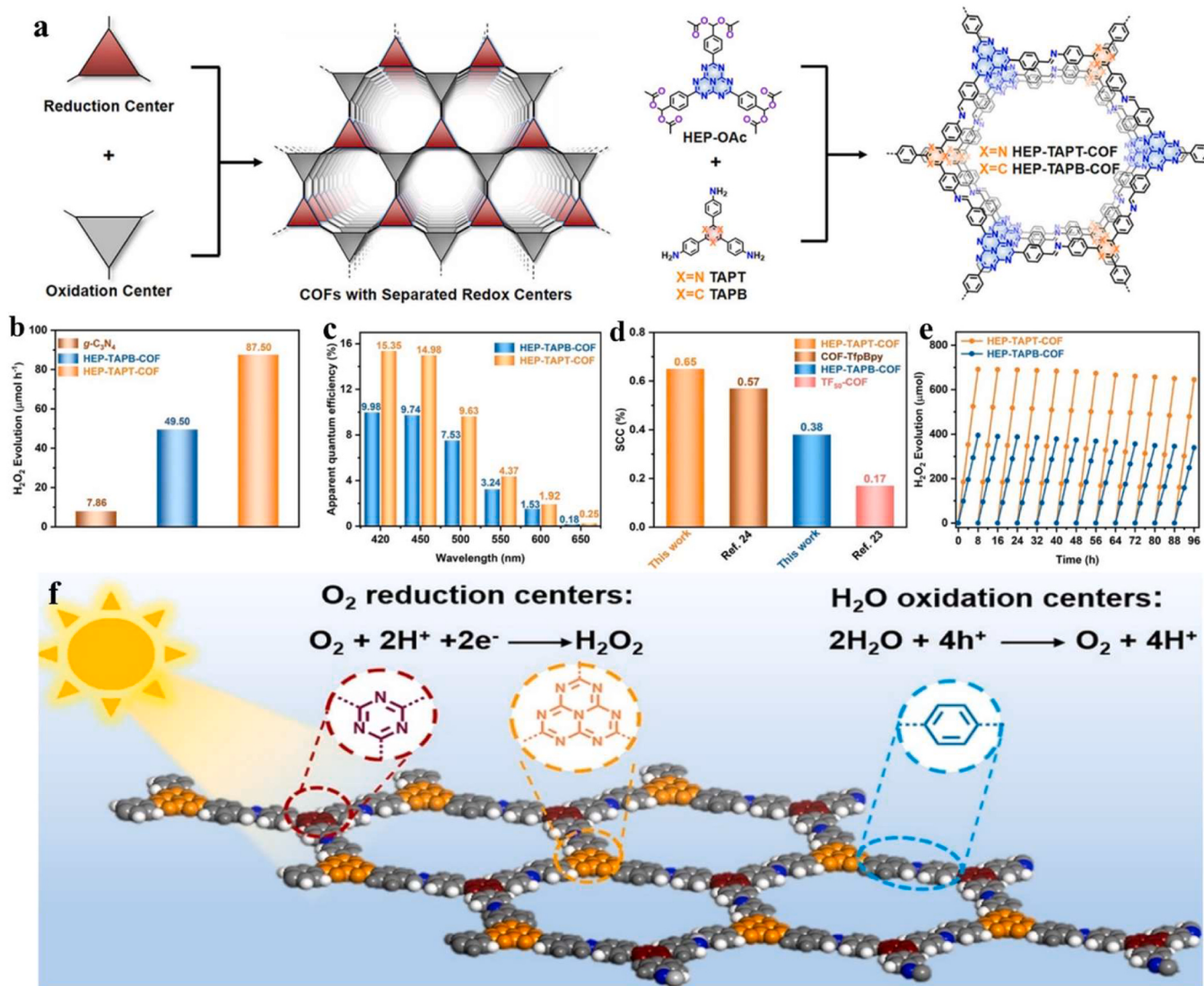


Fig. 14. The schematic illustration of COFs with separated redox centers and synthetic routes of HEP-TAPT-COF and HEP-TAPB-COF (a); photocatalytic H_2O_2 production rates of HEP-COFs and $\text{g-C}_3\text{N}_4$ (b); wavelength-dependent AQEs of HEP-COFs (c); SCC efficiencies of HEP-COFs and other reported COF photocatalysts (d); photocatalytic cycle of HEP-COFs (e); schematic diagram of photocatalytic generation of H_2O_2 with HEP-TAPT-COF as photocatalyst (f). Copyright 2023 Wiley-VCH.

Adapted with permission from ref 142.

H_2O_2 production reaction. Based on the above analysis, $\text{g-C}_3\text{N}_4$ -based heterojunctions are constructed mainly from the perspectives of introducing active sites and improving oxidation capacity of valence band.

The $\text{g-C}_3\text{N}_4$ -based heterojunctions are a complex hybrid of $\text{g-C}_3\text{N}_4$ and other materials with good conductivity and high selectivity for oxygen reduction to H_2O_2 , such as precious metal Au [110], transition metal Cu [108], carbon materials (carbon nanotubes, graphene, porous carbon, etc.) and MXene [115–117]. In the process of H_2O_2 production by oxygen reduction, the photo-generated electrons on $\text{g-C}_3\text{N}_4$ will be transferred to the surface of metal (or carbon materials and MXene) under the action of an internal electric field to react with O_2 [116,117]. At the same time, the hot electrons produced by plasmonic resonance on the metal surface can also reverse transition to the $\text{g-C}_3\text{N}_4$ conduction band, which increases the number of photogenerated electrons involved in oxygen reduction reaction and widens the light absorption range of $\text{g-C}_3\text{N}_4$, thus improving the photocatalytic H_2O_2 production performance of heterojunction.

Inspired by the structure of mussels, Lin et al. prepared a silver-

decorated ultrathin $\text{g-C}_3\text{N}_4$ nanosheets ($\text{Ag}@\text{g-C}_3\text{N}_4\text{-NS}$) heterojunction by Ag nanoparticles modification on the surface of ultra-thin $\text{g-C}_3\text{N}_4$ nanosheets [118]. The larger specific surface area of $\text{g-C}_3\text{N}_4\text{-NS}$ provided more active sites for O_2 reduction reaction. The introduction of Ag nanoparticles expanded the range of light absorption of $\text{g-C}_3\text{N}_4\text{-NS}$ and promoted the effective separation of photogenerated charges in $\text{g-C}_3\text{N}_4\text{-NS}$, then, boosting the efficiency of photocatalytic H_2O_2 production. Accordingly, $\text{Ag}@\text{g-C}_3\text{N}_4\text{-NS}$ showed excellent photocatalytic H_2O_2 production rate ($118.5 \mu\text{mol g}^{-1} \text{h}^{-1}$) in pure water system, which was 4.77 times higher than that of $\text{g-C}_3\text{N}_4\text{-NS}$ ($24.8 \mu\text{mol g}^{-1} \text{h}^{-1}$). Compared with metal materials, carbon materials can not only be comparable in terms of conductivity, but also have the advantages of wide sources, low price, safety and non-toxic. Carbon materials are also commonly used as cocatalysts to improve the photocatalytic performance of $\text{g-C}_3\text{N}_4$. In recent years, hybrid photocatalysts composed of $\text{g-C}_3\text{N}_4$ and carbon materials have been widely used in the field of H_2O_2 production. For example, Shiraishi et al. prepared a carbon-nitride-aromatic diimide-graphene nanohybrids ($\text{g-C}_3\text{N}_4/\text{PDI}/\text{rGO}_{0.05}$) by facile hydro-

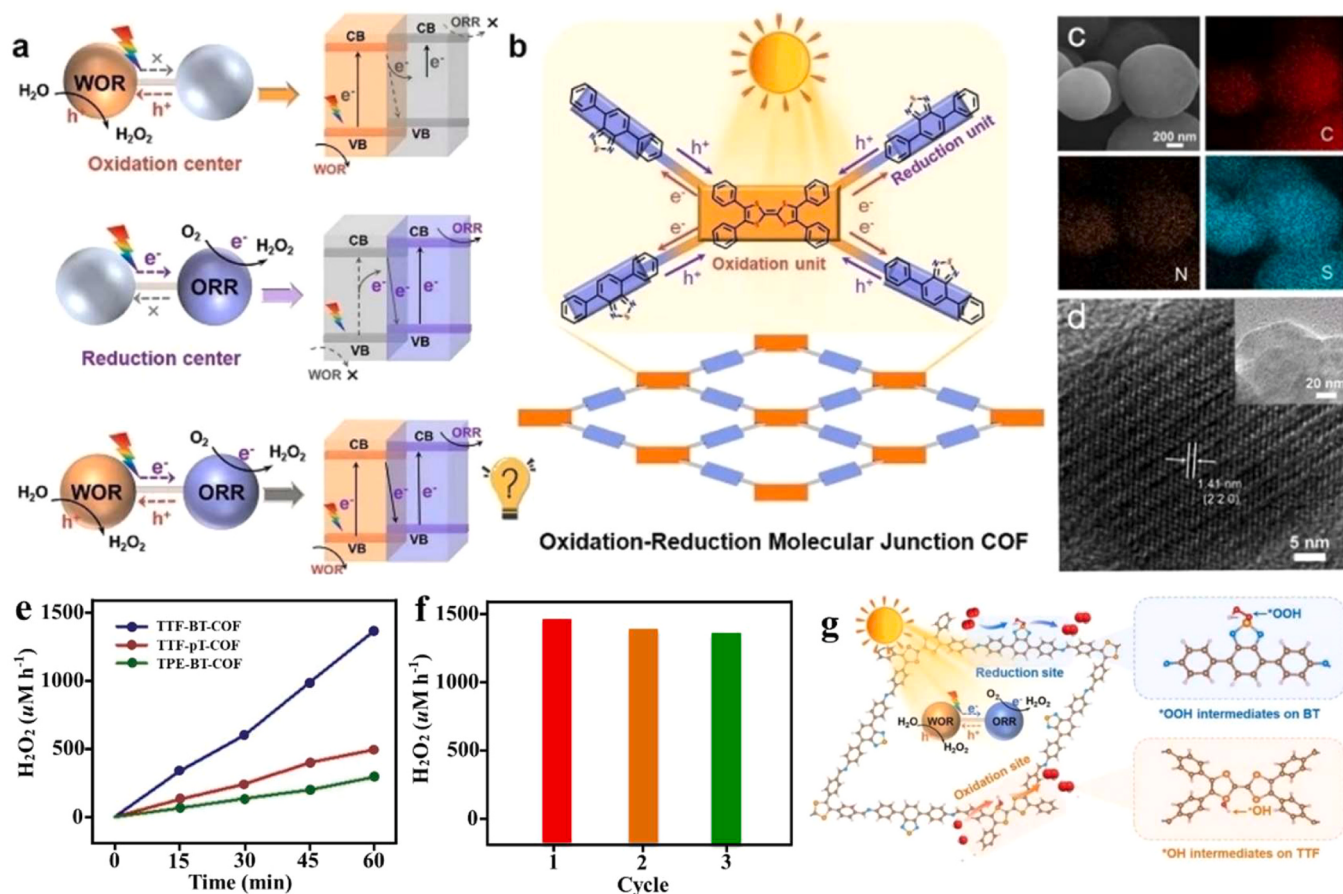


Fig. 15. Schematic illustration of the oxidation-reduction molecular junction COF photocatalyst (a, b); SEM with elemental mapping images (c) and HRTEM image (d) of TTF-BT-COF; time-dependent H₂O₂ generation of TTF-BT-COF, TTF-pI-COF and TPE-BT-COF (e); photocatalytic cycle of TTF-BT-COF (f); adsorption configuration of *OH intermediates on TTF and *OOH intermediates on BT of the TTF-BT-COF (g). Copyright 2023 Wiley-VCH. Adapted with permission from ref 144.

Table 3
Summary of the reported photocatalytic H₂O₂ production by CTFs based photocatalysts.

Photocatalyst	Sacrificial reagent	Irradiation conditions	H ₂ O ₂ activity	AQE	Ref.
CTF-BDBBN	H ₂ O	> 420 nm	97 μmol g ⁻¹ h ⁻¹	-	[148]
CTF-EDBN	H ₂ O	> 420 nm	57 μmol g ⁻¹ h ⁻¹	-	[148]
CTF-BPDCN	H ₂ O	> 420 nm	28 μmol g ⁻¹ h ⁻¹	-	[148]
CHF-BP	H ₂ O	> 420 nm	850 μmol g ⁻¹ h ⁻¹	-	[150]
CHF-DPA	H ₂ O	> 420 nm	1375 μmol g ⁻¹ h ⁻¹	-	[150]
CHF-DPDA	H ₂ O	> 420 nm	1725 μmol g ⁻¹ h ⁻¹	16.0% (420 nm)	[150]
CTF-NS-5BT	H ₂ O: benzyl alcohol (9:1)	≥ 420 nm	1630 μmol g ⁻¹ h ⁻¹	6.6% (420 nm)	[149]
Bpt-CTF	H ₂ O	350–780 nm	3268.1 μmol g ⁻¹ h ⁻¹	8.6% (420 nm)	[151]
Bpu-CTF	H ₂ O	350–780 nm	1353 μmol g ⁻¹ h ⁻¹	-	[151]
Dc-CTF	H ₂ O	350–780 nm	322.2 μmol g ⁻¹ h ⁻¹	-	[151]
CsPbBr ₃ /CTF-2	H ₂ O	420 nm	134.6 μM h ⁻¹	9.98% (420 nm)	[152]
CDS@CTFs	H ₂ O	Simulated sunlight	535.41 μmol g ⁻¹ h ⁻¹	-	[153]

thermal-calcination (Fig. 8a) [119]. The semiconducting g-C₃N₄/PDI moieties could transfer their CB electrons to absorbed O₂ molecules by graphene conductive medium, which improved photo-induced charges separation and two-electron O₂ reduction under the irradiation of visible light. Meanwhile, the VB holes located on the semiconducting moieties oxidized water. It should be mentioned that the activity was much related with rGO hybridization amount, g-C₃N₄/PDI/rGO_{0.05} gave rise to the largest H₂O₂ production, which was much higher than that of g-C₃N₄/PDI without rGO. However, the activity decreased when the rGO loading amount was larger than 0.05% (Fig. 8a). The H₂O₂ generation rate of g-C₃N₄/PDI/rGO_{0.05} remained almost constant with the extension of

photoirradiation time, indicating that the catalyst possessed excellent stability (Fig. 8c). In general, the rational design of g-C₃N₄/PDI/rGO_{0.05} hybrid enhances CB e⁻ transfer from photo-excited g-C₃N₄/PDI to O₂ molecules, and subsequent facilitates H₂O₂ production (Fig. 8d).

4.2. Photocatalytic H₂O₂ production by covalent organic frameworks (COFs)

Covalent organic frameworks (COFs) are a class of porous organic polymers with crystalline and periodic structures [120]. The preparation of COFs is usually based on reversible chemical reactions, such as

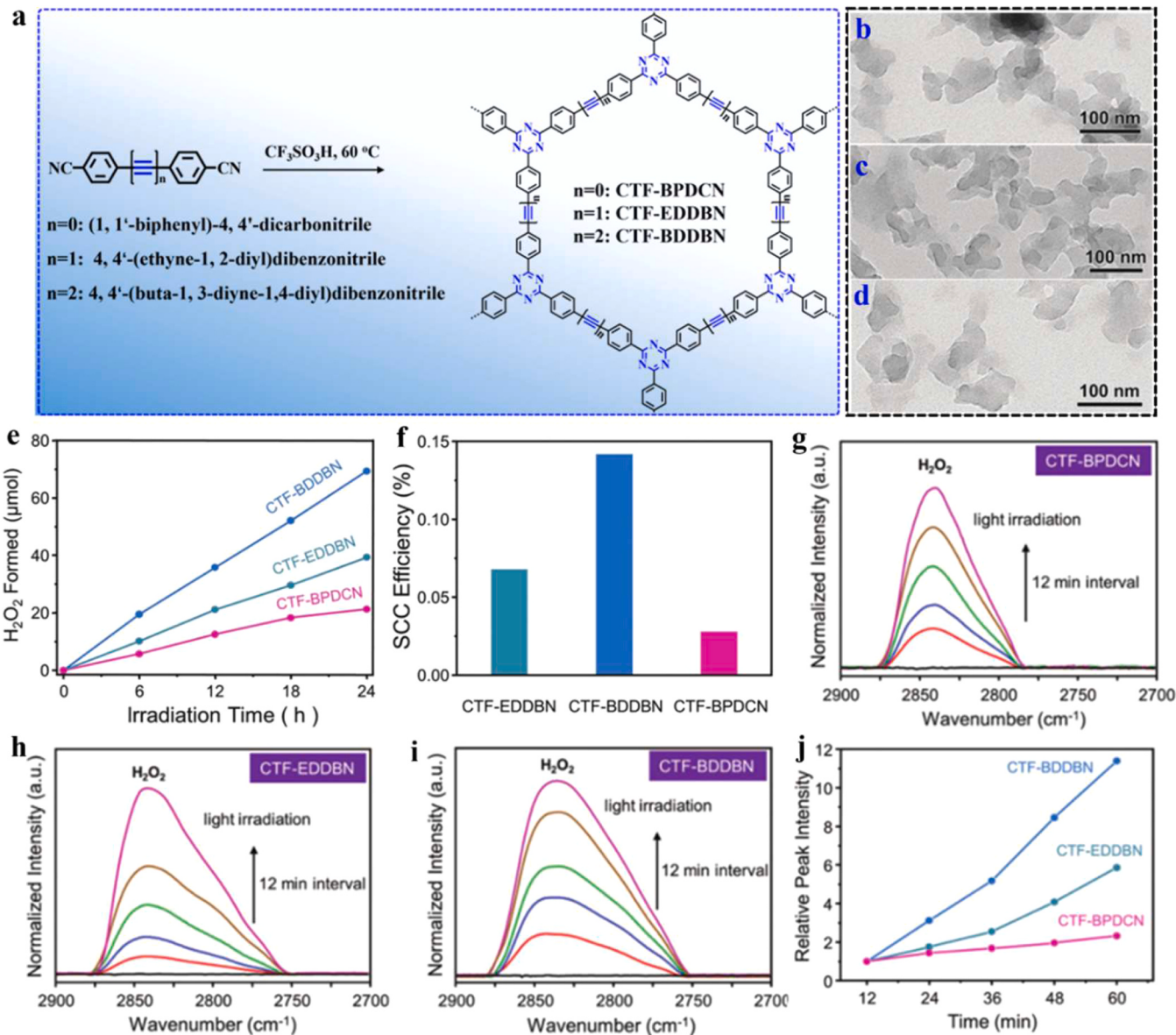


Fig. 16. The schematic illustration of CTF-BPDCN, CTF-EDDBN and CTF-BDDBN (a); TEM images of CTF-BPDCN (b), CTF-EDDBN (c) and CTF-BDDBN(d); time-dependent H_2O_2 generation (e) and SCC efficiencies (f) of CTF-BPDCN, CTF-EDDBN and CTF-BDDBN; In situ DRIFTS of CTF-BPDCN (g), CTF-EDDBN (h) and CTF-BDDBN (i); Time-dependent variations of normalized relative peak intensities as shown in figure g-i (j). Copyright 2020 Wiley-VCH.

Adapted with permission from ref 148.

boronine, boronate-ester, imide, hydrazone, phenazine, enamine and imidazole etc to form reaction [121]. Since Yaghi's research group first reported COF-1 and COF-5 by reversible borate esterification reaction in 2005 [122], the COFs materials have aroused strong research interest due to their unified structural characteristics and great potential in the field of chemistry and materials science [120].

The COFs with semiconductor properties are one of the promising photocatalytic materials because of their large surface area, high hydrothermal stability, low skeleton density, extensive π -delocalization, flexible synthetic strategy and ready functionality [123–131]. The extensive π -delocalization within COFs extended covalent system contributes to visible light harvesting [132]. The π -stacking interactions benefit the migration and transport of carriers along COFs framework and stacking directions, which can prevent the recombination of photo-induced electrons/holes and maximize photocatalytic efficiency [133]. The high surface area can expose more active sites and enhance the accessibility of substrate molecules. More important, the synthesis

mode modules provide rich options for photo-electric and physical properties tailor at the molecular level by integrating suitable building blocks [134,135]. These unique properties have endowed them satisfactory employment in photocatalytic H_2O_2 production, and many of them have exhibited more desirable photocatalytic performances than inorganic semiconductors. Table 2 summarizes the recently reported photocatalytic H_2O_2 production by COFs based materials. In 2020, P. V. D. Voort et al. reported two COFs [TAPD-(Me)₂, TAPD-(OMe)₂] with strong absorption in the range of visible-light and high thermo-chemical stability (Fig. 9a), which were first applied to the photocatalytic generation of H_2O_2 by O_2 reduction [136]. Meanwhile, they exhibited effective charges transfer and separation because of the high crystallinity and large specific surface area as high as $1165 \text{ m}^2 \text{ g}^{-1}$. On the basis of linkers symmetry, the structure models of TAPD-(Me)₂ and TAPD-(OMe)₂ COFs were built through producing the prospective two dimensional kgm topology layers and stacking sequences with overlapping (AA) and interleaved (AB) permutations were used for modeling

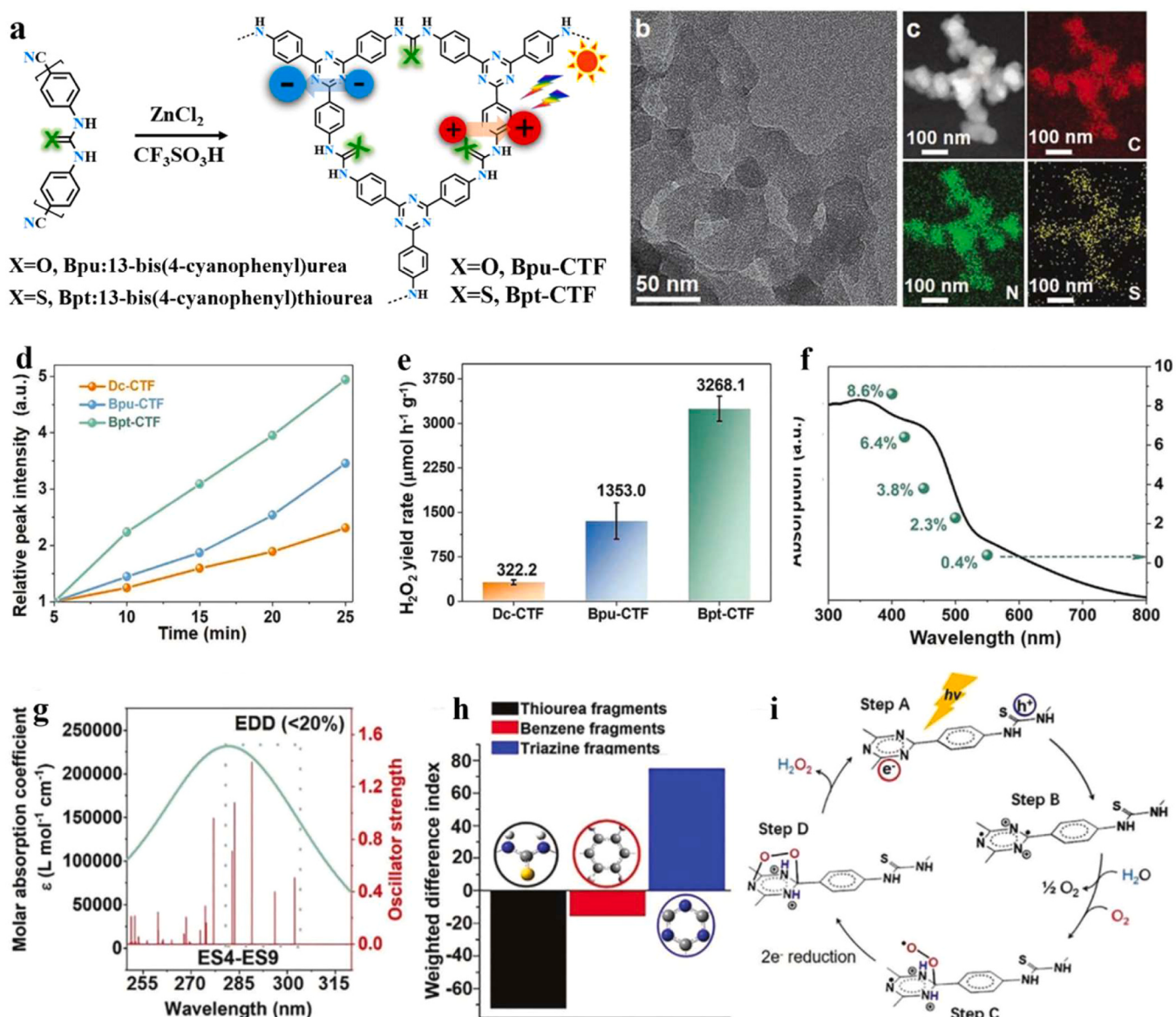


Fig. 17. The schematic illustration of Bpu-CTF and Bpt-CTF (a); TEM image (b) and HAADF-STEM image with corresponding elemental mappings (c) of Bpt-CTF; Time-dependent OH bending intensity (d) and photocatalytic H_2O_2 production (e) for Dc-CTF, Bpu-CTF, and Bpt-CTF; wavelength-dependent H_2O_2 production of Bpt-CTF (f); TDDFT-calculated absorption spectra for electron distribution density (EDD) of Bpt-CTF (g); weight difference index of fragments in excited Bpt-CTF (h); mechanism of photocatalytic H_2O_2 production by Bpt-CTF (i). Copyright 2022 Wiley-VCH.

Adapted with permission from ref 151.

(Fig. 9b,c). Owing to the band gaps of two COFs meeting the requirement of reducing O_2 to H_2O_2 (Fig. 9d,e), they were able to be used for photocatalytic H_2O_2 production. The diaromatic amine (donor) unit facilitates strong performance of reduction, allowing these COFs to effectively reduce O_2 to generate H_2O_2 with a high production rate (Fig. 9f). This research creates a new way for efficient photocatalytic solar energy conversion by using the metal-free, recyclable photocatalytic systems.

Due to the low efficiency of intrinsic charge generation, rapid photo-generated charges recombination, and limited electron transport along the framework, the activity of COFs for photocatalytic generation of H_2O_2 still needs to be improved. Mi et al. first incorporated triazine and acetylene moieties into COFs, synthesizing two vinylene linked COFs (symbolized as EBA-COF and BTEA-COF) for generating H_2O_2 by photocatalysis (Fig. 10a) [137]. The space-separated triazine and acetylene units results in effective charges separation and suppressing their recombination, and the linkage of C=C is conducive to the electrons

transport on the skeletons. For the stacking modes of two COFs, overlapping AA stacking is well matched with the intensity of peaks in the Powder X-ray Diffraction (PXRD) pattern (Fig. 10b-e). The results of experiment and calculation both indicated that the building units of triazine and acetylene synergistically facilitated the synthesis of H_2O_2 via the two-electron path. EBA-COF exhibited high production activity of H_2O_2 and the rate was up to $1830 \mu\text{mol g}^{-1} \text{h}^{-1}$ under the illumination of 420 nm Light Emitting Diode (LED) (Fig. 10f,k), which was better than that of most other COFs photocatalysts. The better photocatalytic performance of EBA-COF for H_2O_2 production is due to its spatial structure characteristics, which is conducive to photo-induced charges separation with faster photo-response (Fig. 10g). The more efficient charges separation of EBA-COF was further demonstrated by photo-luminescence (PL) and electrochemical impedance spectroscopy (EIS) spectra (Fig. 10h,i). The apparent quantum efficiency (AQE) of EBA-COF was measured under the irradiation of 420, 450, 520 and 600 nm, respectively, and the AQE was 4.4% at 420 nm (Fig. 10j). The

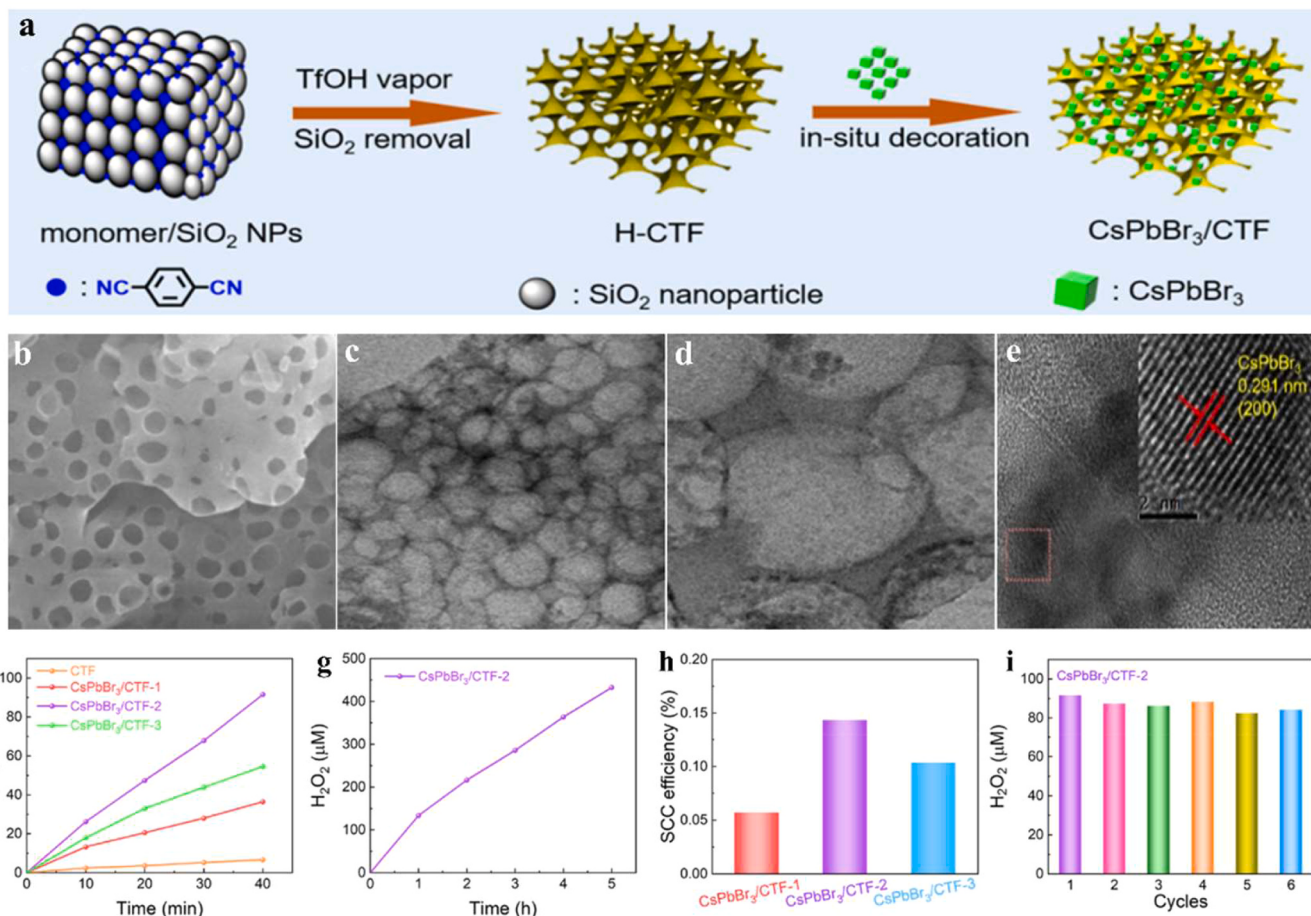


Fig. 18. The schematic illustration of CsPbBr₃/CTFs (a); SEM images (a) and TEM images (c-e) of CsPbBr₃/CTF-2; time-dependent photocatalytic H₂O₂ production of CsPbBr₃/CTFs and CTF-1 (f); time-dependent photocatalytic H₂O₂ production of CsPbBr₃/CTF-2 for 5 h (g); SCC efficiencies of CsPbBr₃/CTFs (h); photocatalytic recycle of CsPbBr₃/CTF-2 (i). Copyright 2022 Elsevier.

Adapted with permission from ref 152.

photoactivity of EBA-COF for H₂O₂ generation did not decrease significantly after 5 consecutive tests, indicating that it had good stability (Fig. 10l). The production of H₂O₂ was investigated by testing the generation rate of H₂O₂ in different sacrificial reagents (Fig. 10m), suggesting that BnOH was the most efficient sacrificial reagent and provided the highest H₂O₂ generation rate of 2550 μmol g⁻¹ h⁻¹. This research provides a novel idea for the design of vinylene-linked COFs with synergistic photocatalytic active sites for producing H₂O₂ under visible-light driven.

Generating H₂O₂ through the photocatalytic reaction between H₂O and O₂ is a desirable approach to efficiently produce this product on a small scale. But the photocatalytic H₂O₂ production efficiency is deeply restricted, owing to the low activity and selectivity of the two-electron H₂O oxidation reaction. In 2022, Ma et al. prepared a new bipyridine-based COF photocatalyst (COF-TfpBpy), which exhibited efficient photocatalytic generation of H₂O₂ from the reaction of H₂O and O₂ with the absence of sacrificial reagents and stabilizers, and the conversion efficiency of solar to chemical energy at 298 K (0.57%) and 333 K (1.08%) were higher than the highest values reported so far [138]. At the same time, the prepared H₂O₂ solution is able to be directly employed to remove pollutants and disinfect water. To determine which monomer in COF-TfpBpy was the active site, the bipyridine monomer was replaced by different monomers to obtain various COFs materials (Fig. 11a-g), and their properties of photocatalytic production of H₂O₂ were investigated (Fig. 11h). The results showed that their activities and the concentrations of H₂O₂ obtained were significantly lower than that of COF-TfpBpy (1042 μM). The mechanism study disclosed that the

outstanding photocatalytic activity of COF-TfpBpy was owing to the bipyridine monomer protonation, which boosted the rate-determined reaction (oxidation reaction of two-electron water), enhancing Yeager-type O₂ adsorption for accelerating O₂ reduction with two-electron one-step. This work firstly proved that COF catalyzed the reaction of water and air to synthesize H₂O₂ under light driven, and paved the way for the treatment of wastewater with H₂O₂ solution prepared by photocatalysis.

Han et al. developed a partial fluorination, metal free and imine-linked 2D triazine COF (TF₅₀-COF) (Fig. 12a) for H₂O₂ generation with photocatalysis [139]. The F-substitution produced a large number of Lewis acid sites, which adjusted adjacent carbons electronic distribution and offered high active sites for O₂ adsorption, broadened the range of visible light response for photocatalyst, thus improving photo-generated charges separation. DFT calculations forecasted that F substitution enhanced π electron interactions, improved the crystallinity and porosity, and was beneficial for photogenerated charges transfer. According to transmission electron microscopy (TEM) images analysis, the interlayer interaction in TF₅₀-COF was maximized by changing the ratio of F, so the crystallinity could be improved with faster carriers transfer and robust light stability (Fig. 12b,c). Meanwhile, TF₅₀-COF photocatalyst exhibited high selectivity and stability for H₂O₂ production via 2e⁻ O₂ photo-reduction, and the yield rate of H₂O₂ was up to 1739 μmol g⁻¹ h⁻¹ under the illumination of visible-light and the prominent apparent quantum efficiency was as high as 5.1% at 400 nm (Fig. 12d-g), which exceeded the previously reported performance of COF-based photocatalysts with non-metal. This partial fluorination

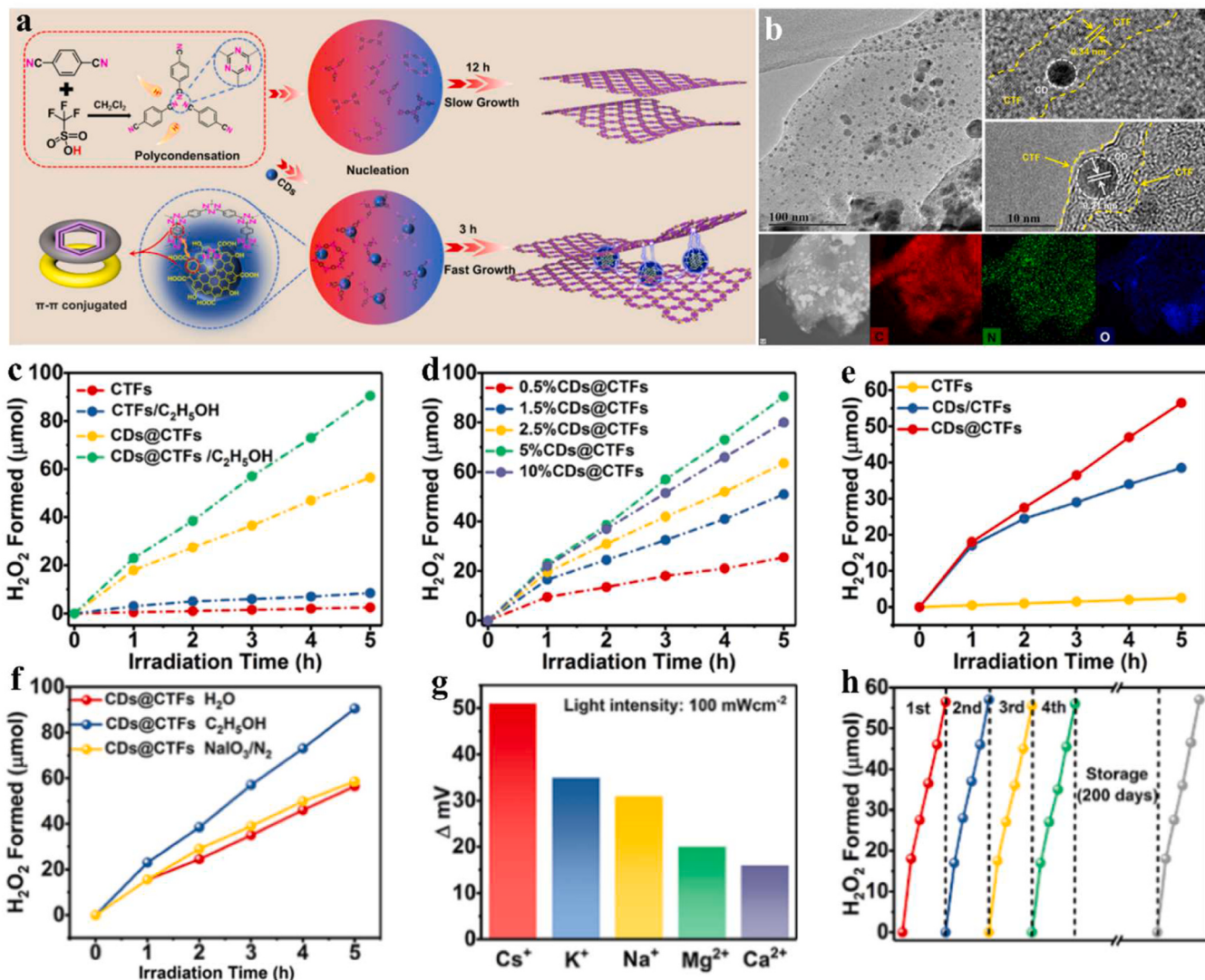


Fig. 19. The schematic illustration of CTFs and CDs@CTFs (a); TEM image, HRTEM images and STEM-EDS mapping of CDs@CTFs (b); Photocatalytic H₂O₂ production of CTFs and CDs@CTFs before and after adding ethanol sacrifice agent (c); activity comparison of CDs@CTFs with different amounts of CDs (d); of CTFs, CDs/CTFs and CDs@CTFs (e); photocatalytic H₂O₂ production for of CDs@CTFs with various scavengers (f); surface voltage variations of CDs@CTFs in the solution containing different alkali metal ions (g); photocatalytic recycle of CDs@CTFs (h). Copyright 2023 Elsevier.

Adapted with permission from ref 153.

strategy provides a powerful tool kit for further designing triazine COFs for effective and stable solar-to-chemical energy conversion (SCC).

H₂O₂ is a significant chemical that can be used for industrial production on a large scale, and its production has attracted extensive attention. COFs materials have been certified to be an excellent platform for photocatalytic H₂O₂ production. In 2022, Chen et al. fabricated two 2D COFs (N₀-COF and N₃-COF) with high crystallinity for photocatalytic generation of H₂O₂ through the synthetic route shown in Fig. 13a-c [140]. Not only N₀-COF but also N₃-COF is active for H₂O₂ generation by using H₂O and O₂ as reactive materials under visible light illumination in the absence of any other sacrificial agent. However, the two COFs exhibited distinct differences in performance, which could be interpreted for the existence of donor-receptor configurations in the framework. N₀-COF in contrast to its nitrogen-containing analogue N₃-COF has higher charge separation efficiency and better band alignment, leading to the production rate of H₂O₂ (15.7 μmol h⁻¹) for N₀-COF 10 times higher than that of N₃-COF (Fig. 13d). The photocatalytic production of H₂O₂ under different atmospheres was also evaluated, N₀-COF provided the highest H₂O₂ production rate under pure O₂ atmosphere, which significantly suppressed under air, and completely

inhibited under Ar (Fig. 13e). This resultant suggested that H₂O₂ was produced via the two-electron O₂ reduction. The effect of irradiation wavelengths on H₂O₂ production of N₀-COF exhibits desirable photoactivity in a broad range light absorption (Fig. 13f). In addition, the stability of N₀-COF was assessed via cyclic tests (Fig. 13g), and there was no obvious decrease in the generation yield of H₂O₂ for five cycles. The relationship of property and structure was studied by experiment and calculation methods. The improvement in performance is mainly attributed to form the donor-receptor structure, as it not only promotes the photo-excited charges separation, but also effects the active sites to make up for the energy barriers. This research supplies a new way to rationally design metal free photocatalysts for photocatalytic H₂O₂ evolution. Tong et al. used suitable amounts of phenyl groups as electron donors to achieve optimal intramolecular polarity of COFs, which could maximize the free charge generation for H₂O₂ photosynthesis under light irradiation without sacrificial agents [141].

It is highly desirable for COFs to achieve efficient whole H₂O₂ photosynthesis through the design of molecular. However, the precise construction of COFs for producing H₂O₂ via photosynthesis is still a huge challenge. In 2022, Chen et al. prepared two novel COFs (labeled as

Table 4Summary of the reported photocatalytic H₂O₂ production by COPs based photocatalysts.

Photocatalyst	Sacrificial reagent	Irradiation conditions	H ₂ O ₂ activity	AQE	Ref.
DE7-M	H ₂ O	> 420 nm	266 μmol (24 h)	8.7% (420 nm)	[170]
TPE-AQ	H ₂ O	> 400 nm	909 μmol g ⁻¹ h ⁻¹	-	[171]
TPE-AC	H ₂ O	> 400 nm	293 μmol g ⁻¹ h ⁻¹	-	[171]
NMT350	H ₂ O	AM 1.5 G	119.6 μmol g ⁻¹ h ⁻¹	-	[167]
NMT400	H ₂ O	AM 1.5 G	270.9 μmol g ⁻¹ h ⁻¹	2.6% (420 nm)	[167]
NMT450	H ₂ O	AM 1.5 G	174.2 μmol g ⁻¹ h ⁻¹	-	[167]
AMT400	H ₂ O	AM 1.5 G	83.6 μmol g ⁻¹ h ⁻¹	-	[167]
MNMT400	H ₂ O	AM 1.5 G	75.1 μmol g ⁻¹ h ⁻¹	-	[167]
HMP-PPR	H ₂ O:IPA (8:2)	> 420 nm	31.25 μmol g ⁻¹ h ⁻¹	0.35% (400 nm)	[168]
TPT-alkynyl-AQ	H ₂ O	> 400 nm	2368 μmol g ⁻¹ h ⁻¹	25% (450 nm)	[165]
TPT-AQ	H ₂ O	> 400 nm	1184 μmol g ⁻¹ h ⁻¹	-	[165]
TPT-imine-AQ	H ₂ O	> 400 nm	473.6 μmol g ⁻¹ h ⁻¹	-	[165]
PQTEE-COP	H ₂ O	≥ 400 nm	3009 μmol g ⁻¹ h ⁻¹	3.37% (400 nm)	[164]
BPTEE-COP	H ₂ O	≥ 400 nm	982 μmol g ⁻¹ h ⁻¹	1.10% (400 nm)	[164]
AQTEE-COP	H ₂ O	≥ 400 nm	3204 μmol g ⁻¹ h ⁻¹	3.59% (400 nm)	[172]
NATEE-COP	H ₂ O	≥ 400 nm	1265 μmol g ⁻¹ h ⁻¹	1.42% (400 nm)	[172]
CP-3	H ₂ O	420–750 nm	133 μmol g ⁻¹ h ⁻¹	8.4% (450 nm)	[169]
AQTT-COP	H ₂ O	≥ 400 nm	3221 μmol g ⁻¹ h ⁻¹	-	[173]
AQTB-COP	H ₂ O	≥ 400 nm	1436 μmol g ⁻¹ h ⁻¹	-	[173]

HEP-TAPT-COF and HEP-TAPB-COF) through the condensation of s-heptazine including HEP-OAc monomer with TAPT [1,3,5-tris(4-aminophenyl)triazine] and TAPB [1,3,5-tris(4-aminophenyl)benzene], respectively (Fig. 14a), which integrated the units of triazine and benzene to COFs framework, remarkably improved the photocatalytic performance for H₂O₂ production [142]. The embedded s-heptazine unit and benzene group in HEP-TAPB-COF serve as the reaction sites of O₂ reduction and H₂O oxidation, respectively. On the contrary, s-heptazine and triazine groups in HEP-TAPT-COF both serve as the reaction sites of O₂ reduction, while phenyl groups serve as the centers of H₂O oxidation. The spatially ordered separation of active sites in HEP-COFs are able to effectively facilitate charges separation and inhibit charges recombination, thus improving the photocatalytic activity of H₂O₂ generation. In comparison with HEP-TAPB-COF, HEP-TAPT-COF with s-heptazine and triazine groups double active centers of oxygen reduction demonstrated higher H₂O₂ generation yield of 87.50 μmol h⁻¹ (Fig. 14b). In addition, HEP-TAPT-COF exhibits a significant higher solar-chemical energy conversion efficiency (0.65%) (Fig. 14c) and a higher apparent quantum efficiency (15.35%) (Fig. 14d) at 420 nm, exceeding HEP-TAPB-COF and that of previously reported COFs-based photocatalysts, which further demonstrates that spatially separated redox centers in the HEP-TAPT-COF framework is able to improve the photocatalytic activity of H₂O₂ preparation. It can be seen from Fig. 14e, the photocatalytic yields of H₂O₂ generation for HEP-TAPB-COF and HEP-TAPT-COF did not attenuate significantly after photocatalysis for 96 h, indicating that they have outstanding stability. According to the results of above experiments and calculations, the entire photocatalytic process of HEP-COFs was summarized (Fig. 14f). In HEP-TAPT-COF, the double active centers composed of s-heptazine and triazine can undergo the double-electron oxygen reduction reaction, but in HEP-TAPB-COF, only the s-heptazine part is able to generate H₂O₂. At the same time, the four-electron water oxidation reactions of the two HEP-COFs occur on the benzene ring. This study provides a new strategy to rationally design polymer-based photocatalysts for the synthesis of efficient solar-driven fuels.

In order to maximize the utilization of light and conquer the tanglesome reaction process of anthraquinone oxidation, H₂O₂ is highly required to achieve total reaction photosynthesis with the combination of H₂O oxidation and O₂ reduction in the absence of sacrificial agents [143]. Lan et al. synthesized a novel COF (TTF-BT-COF) via the covalent coupling reaction between tetrafluoropentene as photooxidation site and benzothiazole as photoreduction site, which exhibited visible light adsorption zone, effective separation efficiency of electrons and holes, and photoredox sites, thus achieving the preparation of H₂O₂ by photocatalytic total reaction (Fig. 15a,b) with the high generation rate of

276000 μM h⁻¹ g⁻¹ [144]. According to SEM, the morphology of TTF-BT-COF was characterized. The results indicate that TTF-BT-COF is consisted of full spheres with the diameter between 400 ~ 600 nm. Besides, EDS analysis indicates that C, N, S are equally distributed on TTF-BT-COF (Fig. 15c). The fast fourier transform image of HR-TEM (high resolution transmission electron microscopy) showed the arrangement of hexagonal structure along the (100) crystal axis of the pores, which was able to demonstrate the AA stacking mode of the two-dimensional TTF-BT-COF structure (Fig. 15d). In comparison with TTF-pT-COF and TPE-BT-COF, the amount of H₂O₂ produced by TTF-BT-COF photocatalysis was more (Fig. 15e), which was attributed to the molecular junction of oxidation-reduction established in TTF-BT-COF. Furthermore, the photocatalytic performance of TTF-BT-COF remained basically unvaried for 3 cycles and the H₂O₂ yield remained stable, which certified the high cyclic stability of TTF-BT-COF (Fig. 15f). In Fig. 15g, a beneficial photosynthesis of hydrogen peroxide mechanism is proposed, that is the formation of REDOX molecular junction in TTF-BT-COF, which is able to facilitate electron-hole pairs separation and greatly lower the energy barrier of water oxidation reaction (WOR) and ORR, making the electrons be captured by O₂ and H₂O much easier and utilizing the holes to form active intermediates, producing H₂O₂ ultimately. This is the first time to design the molecular junction of oxidation-reduction COF for the total reaction photosynthesis of hydrogen peroxide, which may broaden the applications of COFs in H₂O₂ generation.

4.3. Photocatalytic H₂O₂ production by covalent triazine frameworks (CTFs)

Covalent Triazine Frameworks (CTFs) are a kind of organic porous materials mainly constructed from triazine structural units, which are characterized by high thermal stability, good chemical stability, large specific surface area and rich nitrogen content [145]. The strong covalent bonds (C=N) in CTF materials allow them to show high stability even in strong acids and bases, and the rich nitrogen content in the skeleton structure and the ability to add heteroatoms to the skeleton structure provide the basis for a variety of potential applications [146]. Since Thomas et al. successfully synthesized CTF-1 materials by high dynamic condensation reaction in 2008 [147], which have been widely used in gas adsorption separation, environmental remediation, energy storage and heterogeneous catalysis etc [145].

In recent years, CTFs as metal free photocatalysts have exhibited great potential in photocatalytic production of H₂O₂ through the dual electron reduction of O₂ molecules [148–150]. However, the water two-electron oxidation as the other half reaction is still elusive for the

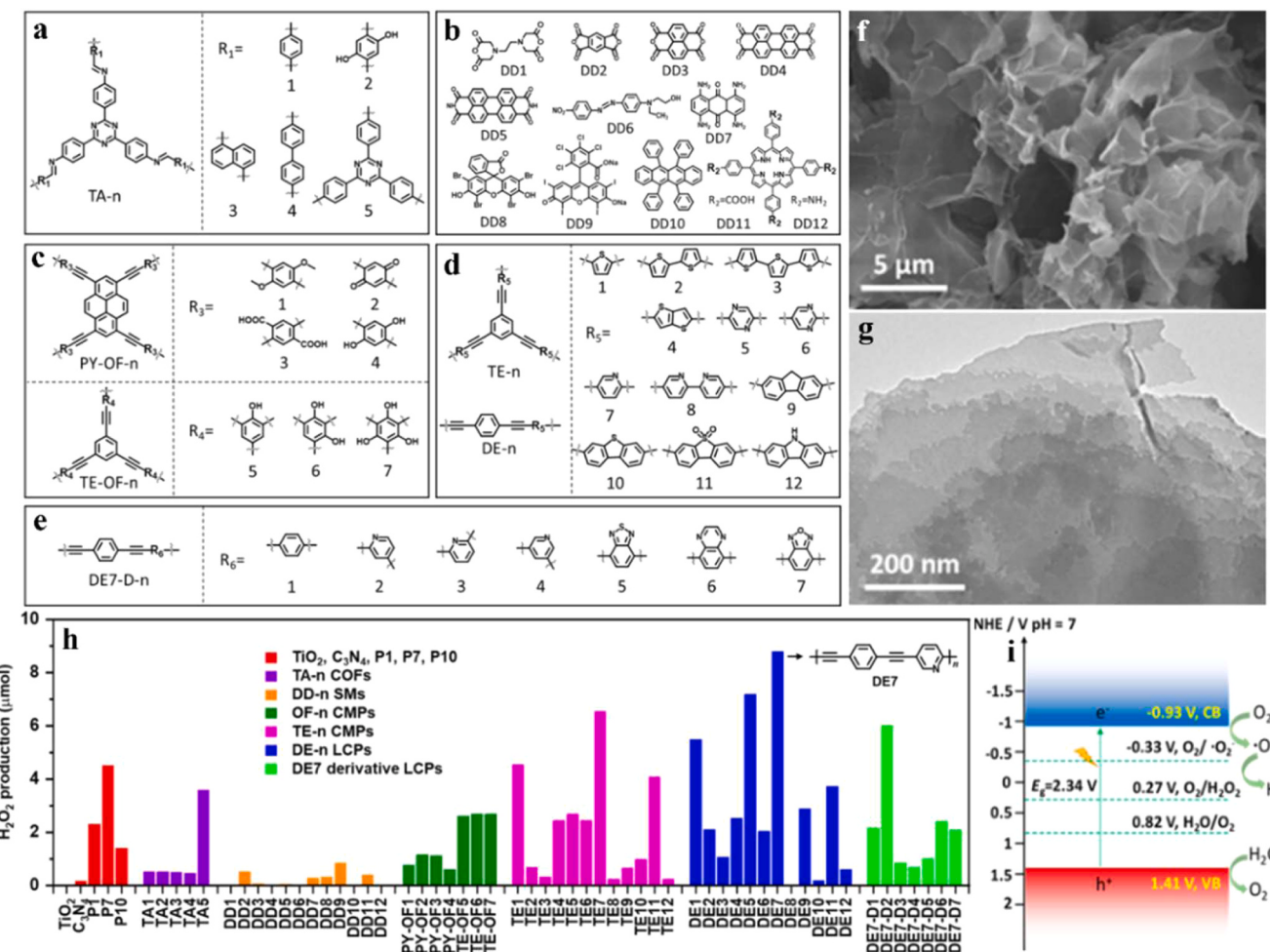


Fig. 20. The structures of TA-n COFs (a), small molecules, DD-n (b), PY/TE-OF-n CMPs (c), TE-n CMPs and DE-n LCPs (d) and DE7 LCP analogues (e); SEM (f) and TEM (g) images of DE7-M; photocatalytic H₂O₂ production of various organic materials (h); calculated energy band positions and proposed mechanism of DE7-M (i). Copyright 2021 American Chemical Society.

Adapted with permission from ref 170.

production of H₂O₂. So enabling this pathway of water oxidation is crucial for improving the yield and maximizing the utilization efficiency of atom. Table 3 summarizes the recently reported photocatalytic H₂O₂ production by CTFs based materials. In 2020, Xu et al. successfully synthesized three novel CTF-based polymer photocatalysts (CTF-BPDCN, CTF-EDDBN and CTF-BDDBN) through the corresponding precursors (Fig. 16a) [148]. As shown in Fig. 16b-d, TEM images show that after liquid phase peeling, ultra-thin nanosheets with a size of hundreds of nanometers can be obtained, which can more effectively use photons for photocatalytic reaction, so that the surface active sites can be completely exposed, and the charges can be effectively separated, ultimately improving the photocatalytic activity. Studies have shown that the introduction of C≡C or C≡C-C≡C group in the CTFs can significantly facilitate the photocatalytic formation of H₂O₂ and the efficiency of atomic utilization is as high as 100%, because acetylene and diacetylene groups are able to obviously reduce the energy connected with OH^{*} formation, thus enabling a new two-electron oxidation pathway to generate H₂O₂. Therefore, the photocatalytic properties of CTF-EDDBN and CTF-BDDBN both including acetylene and diacetylene groups are better and the amounts of H₂O₂ production are more than that of CTF-BPDCN without acetylene and diacetylene groups (Fig. 16e). The SCC efficiency is up to 0.14% by using CTF-BDDBN as photocatalyst, exceeding the global average of ≈ 0.10% for natural synthetic plants (Fig. 16f). According to the in situ diffuse reflectance fourier transform infrared spectroscopy (DRIFTS) for CTF-BPDCN, CTF-EDDBN and

CTF-BDDBN (Fig. 16g-i), which proves that H₂O₂ is formed under light irradiation. In addition, the normalized relative peak intensities of all CTFs at 2848 cm⁻¹ showed that CTF-BDDBN exhibited the fastest growth in the aspect of H₂O₂ formation (Fig. 16j). This study reveals a significant reaction pathway for photocatalytic generation of H₂O₂, which reflects that precise control polymer photocatalysts chemical structures are essential for achieving efficient solar to chemical energy conversion.

The photoreduction of two-electron O₂ to H₂O₂ is severely suppressed by its slow charge dynamics. Han et al. successfully prepared two novel (thio)urea functionalized CTFs (Bpt-CTF and Bpu-CTF), and one unfunctionalized Dc-CTF by reasonable design, exhibiting varied charges separation and transfer capabilities (Fig. 17a) [151]. The strategy of polarization engineering is certified via grafting thiourea functional groups onto CTFs, resulting in distinctly facilitated charges separation/transport and significantly improved protons transfer, thus greatly improving the ability of H₂O and O₂ to produce H₂O₂ through 2e⁻ ORR. The TEM image shows that the morphology of Bpt-CTF is nanosheet (Fig. 17b) and the corresponding elements (C, N, S) contained are proved through the High-Angle Annular Dark Field-Scanning Transmission Electron Microscopy (HAADF-STEM) image (Fig. 17c). As the illumination time increased, all CTFs exhibited a vibration peak corresponding to OH bending at 2820 cm⁻¹, and the intensity of OH bending peak is the strongest in PBT-CTF and the weakest is in Dc-CTF, confirming the generation of H₂O₂ under illumination (Fig. 17d). Moreover,

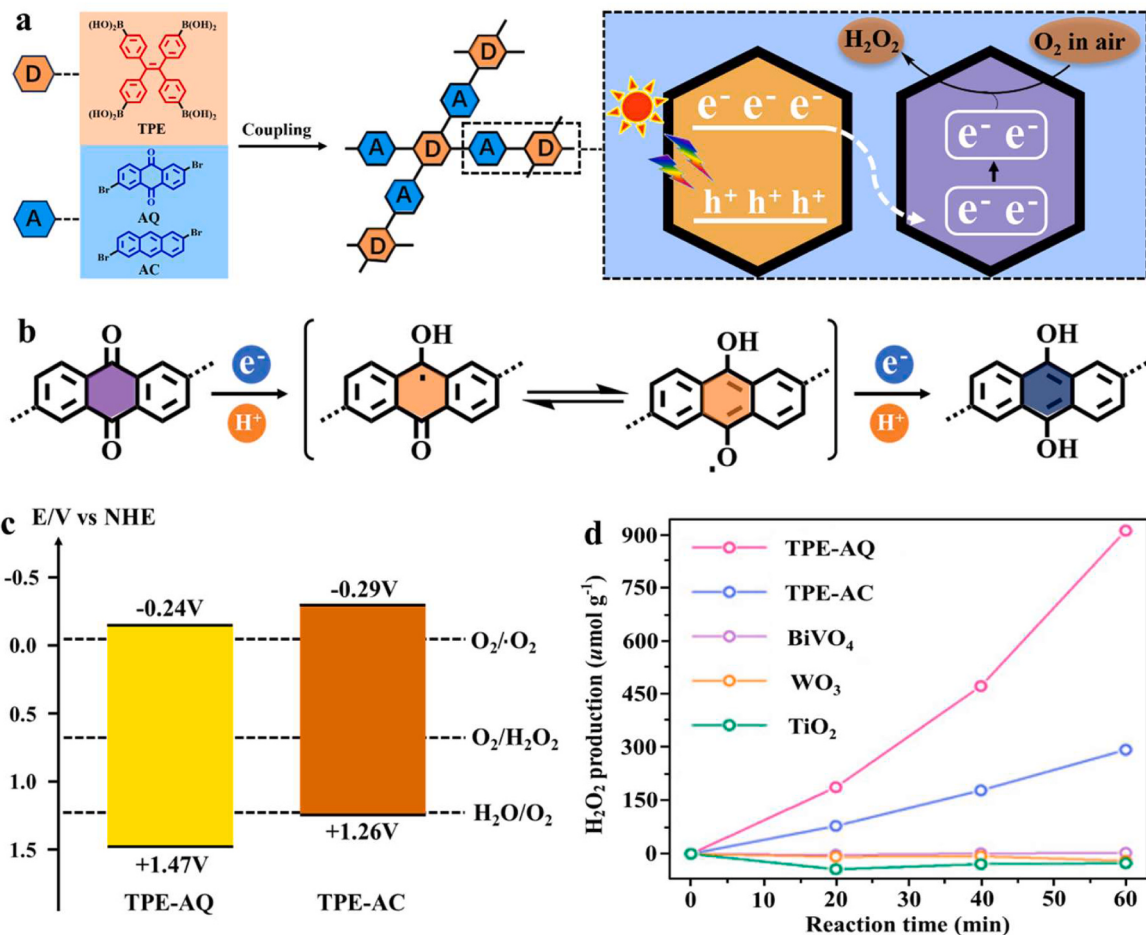


Fig. 21. The synthesis of TPE-AQ and TPE-AC (a); The stepwise electron storing pathway in AQ (b); the electronic energy band structure of TPE-AQ and TPE-AC (c); photocatalytic H_2O_2 production of the frequently studied photocatalysts (d).

the functionalized Bpt-CTF significantly increased the photocatalytic H_2O_2 generation rate to $3268.1 \mu\text{mol h}^{-1} \text{g}^{-1}$ without sacrificial agents or auxiliary catalysts (Fig. 17e), which was an order of magnitude higher than the non-functionalized Dc-CTF, and significantly improved the quantum efficiency (8.6%) at 400 nm (Fig. 17f). The photocatalytic charge kinetics of Dc-CTF, Bpu-CTF and Bpt-CTF were investigated by time-dependent density functional theory (TDDFT) calculation, among them, Bpt-CTF showed the highest excited states (ES) electron and/or hole distribution density (< 20%, Fig. 17g), indicating that the introduction of polar groups can facilitate the accumulation of electrons/holes in N 2p and C=O/C=S groups under photoexcitation. The mechanism of Bpt-CTF photocatalytic preparation of H_2O_2 is shown in Fig. 17i, which reveals the photocatalytic property is due to observably improving two-electron O_2 reduction reaction via the formation of endoperoxides in the triazine reduction site and high concentration holes at the thiourea oxidation site (Fig. 17h). This work offers many opportunities to design high performance metal-free polymer photocatalysts for artificial photosynthesis and environmental remediation at the molecular level.

The artificial photocatalysis technology for H_2O_2 generation holds great promise in addressing growing energy and environmental challenges. CTFs are regarded as a kind of hopeful photocatalysts for H_2O_2 production. Whereas, the photocatalytic performance of single CTF remains unsatisfactory, mainly due to the severe recombination of charges and is short of skillful catalytic sites of O_2 adsorption/activation. Ye et al. fabricated CsPbBr_3 /CTFs nanocomposites with a uniform distribution of active sites via porous CsPbBr_3 in-situ modifying CTFs for improving photocatalytic production of H_2O_2 from O_2 with the absence

of any sacrificial agents (Fig. 18a) [152]. The SEM image of CsPbBr_3 /CTFs exhibited the structure of ordered hollow interconnecting pores with visible diameters of about 230 nm (Fig. 18b), which was able to further be determined by the image of TEM (Fig. 18c). Fig. 18d showed that the distribution of CsPbBr_3 quantum dots on the H-CTFs framework was random. In addition, it can be seen that the CsPbBr_3 quantum dots are in close contact with the H-CTFs framework (Fig. 18e), and the planar spacing of the CsPbBr_3 quantum dots on the (200) crystal plane is 0.291 nm. The above results further demonstrated that CsPbBr_3 /CTFs nanocomposites were successfully prepared. The results of photocatalytic production of H_2O_2 for all samples showed that the activity of CsPbBr_3 /CTF-2 photocatalyst was the highest with a value of $134.6 \mu\text{M h}^{-1}$, which was 13.3 times higher compared with pure CTFs with $10.1 \mu\text{M h}^{-1}$ (Fig. 18f). And CsPbBr_3 /CTF-2 exhibited a high SCC efficiency up to 0.14%, which was higher than that of CsPbBr_3 /CTF-1 and CsPbBr_3 /CTF-3 (Fig. 18h). Besides, a consistent and stable H_2O_2 production of CsPbBr_3 /CTF-2 was observed within five hours (Fig. 18g), and the yield of H_2O_2 generation for CsPbBr_3 /CTF-2 can be maintained well after 6 cycles, indicating the outstanding photocatalytic stability (Fig. 18i). The excellent photocatalytic performance is due to the synergistic effect between CTFs matrix and CsPbBr_3 active quantum dots. This work opens up a path to the development of organic-inorganic nanocomposites for a variety of photocatalytic applications through a highly efficient process.

The incorporation of carbon dots (CDs) to CTFs interlayer is a promising strategy to significantly improve the photocatalytic performance of H_2O_2 production. In 2022, Hu et al. prepared a new type of metal-free hybrid photocatalyst (CDs@CTFs) for efficient photocatalytic

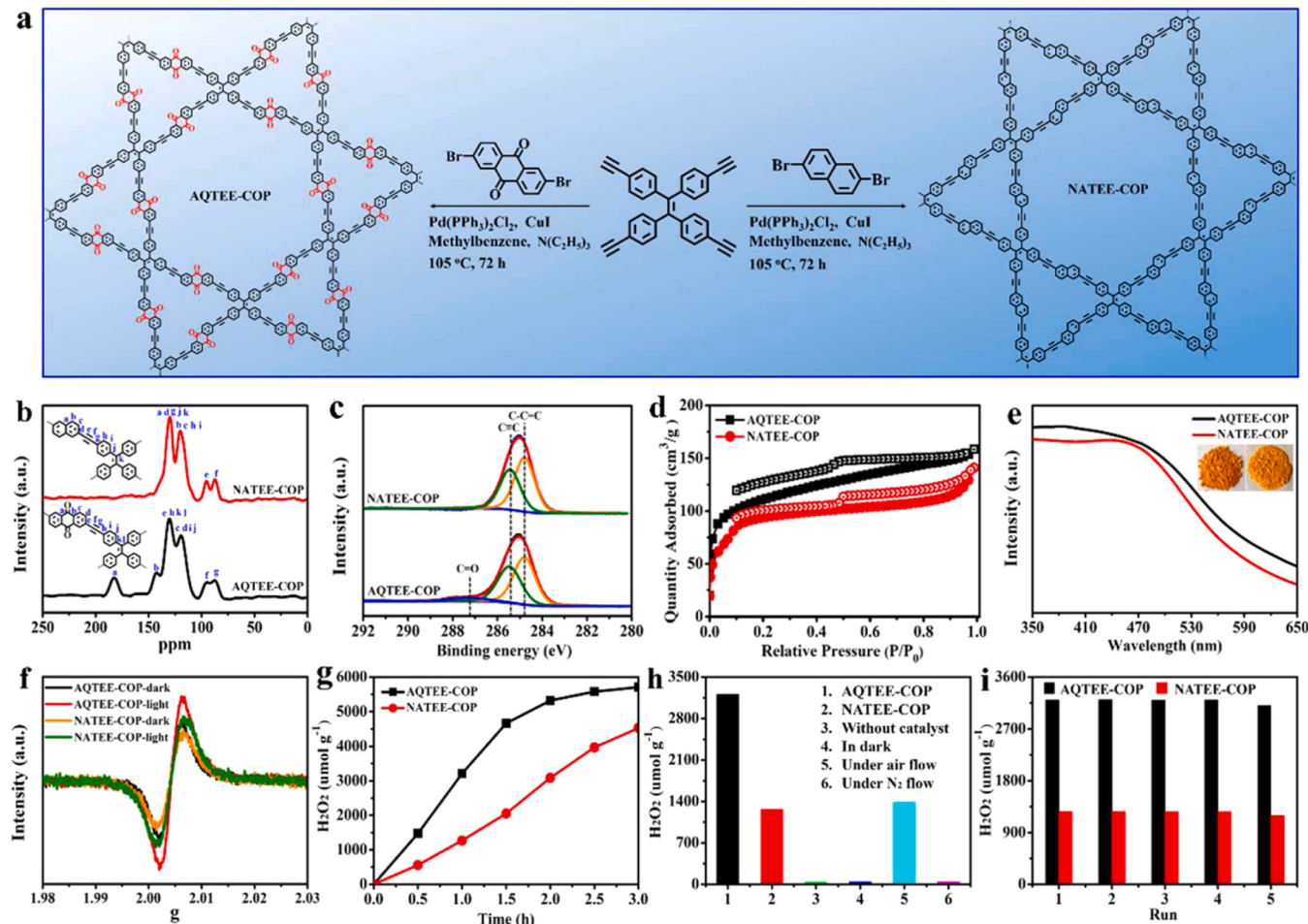


Fig. 22. The schematic synthesis illustration (a), solid state ¹³C NMR spectra (b), N₂ sorption isotherms at 77 K (c), high-resolution C 1 s XPS spectra (d), UV-vis DRS and optical images (e), EPR spectra (f), kinetic profile of H₂O₂ production (g) for AQTEE-COP and NATEE-COP; photocatalytic H₂O₂ production under various conditions (h); photocatalytic recycles of AQTEE-COP and NATEE-COP (i). Copyright 2021 American Chemical Society.

Adapted with permission from ref 172.

H₂O₂ production through incorporating inexpensive and versatile CDs to the interlayer of CTFs (Fig. 19a), as CDs not only facilitate CTFs nucleation and growth, increasing their hourly productivity by 13.5 times, but also form unique hybrid nanoscale sandwich structures with efficient charges separation performance [153]. As shown in Fig. 19b, the images of TEM show that a large number of small nanoparticles are decorated on the ultrathin CTF nanosheets with super large dimensions, and further high-resolution TEM observations reveal that CDs are embedded in CTFs layers or encapsulated by CTFs polymer. The STEM-EDS (Scanning Transmission Electron Microscopy-Energy Dispersive Spectrometer) mapping further proved the uniform distribution of CDs in CTFs, as the O element only originated from CDs. In the absence of sacrificant, the photocatalytic activity of CDs@CTFs is higher with the H₂O₂ generation rate of 22.6 times than that of pure CTFs (Fig. 19c). Fig. 19d shows that incorporate 5 wt% CDs into the preparation system can make CDs@CTFs have the highest H₂O₂ generation rate in the existence of ethanol. Furthermore, the generation yield of H₂O₂ for CDs@CTFs is significantly lower in comparison with CDs@CTFs under the same condition, which means that the structures of CDs@CTFs and CDs/CTFs are varied (Fig. 19e). It can be seen from Fig. 19f that ethanol as a hole sacrificial agent is able to improve the H₂O₂ generation for CDs@CTFs under atmospheric condition. In addition, the CDs-induced surface polarization electric field of CTFs can be modulated by simple adsorption of alkali metal ions to further promote the separation and migration carriers, thus enhancing the H₂O₂ generation efficiency

(Fig. 19g). There was no significant decrease in the generation yield of H₂O₂ (Fig. 19h), which reflects that the designed photocatalyst is highly stable and well reusable. This work provides a new idea for efficient photocatalytic preparation of H₂O₂.

4.4. Photocatalytic H₂O₂ production by covalent organic polymers (COPs)

Covalent organic polymers (COPs) are a class of porous polymers connected by covalent bonds with conjugated frameworks and permanent pore structures [154,155]. The conjugated structural properties that provide electron transport paths enable COPs potential applications in the field of optoelectronics [156,157]. A. I. Cooper et al. reported the first COPs by the reaction of polyterminal alkynyl benzene and halogenated aromatic hydrocarbons in 2007 [158]. Subsequently, researchers have made a lot of efforts in the development and expansion of COPs synthesis methods and construction strategies. At present, the commonly used methods for synthesis of COPs include Suzuki coupling reaction [159], Sonogashira coupling reaction [160], Yamamoto coupling reaction [161], Buchwald-Hartwig (B-H) coupling reaction and oxidation coupling reaction etc [162,163]. The diversification of structural elements and synthesis methods make the preparation of COPs more selective and functional, so COPs have good effects in adsorption, separation, catalysis, sensing, photoelectric and other fields [154].

The photocatalytic synthesis of H₂O₂ from O₂ and H₂O under the

Table 5
The list of abbreviations in the text.

Entry	Full name	Abbreviation
1	Hydrogen peroxide	H ₂ O ₂
2	graphite carbon nitride	g-C ₃ N ₄
3	covalent organic frameworks	COFs
4	covalent triazine frameworks ()	CTFs
5	covalent organic polymers	COPs
6	valence band	VB
7	conduction band	CB
8	versus	vs.
9	Normal Hydrogen Electrode	NHE
10	electron	e ⁻
11	hole	h ⁺
12	biphenyl diimide	BDI
13	pyromellitic diimide	PDI
14	mellitic triimide	MTI
15	anthraquinone	AQ
16	anthraquinone-2-carboxylic acid	AQ-COOH
17	anthrahydroquinone	AQH ₂
18	reference	Ref
19	apparent quantum efficiency	AQE
20	two dimensional covalent organic frameworks	2D-COFs
21	Powder X-ray Diffraction	PXRD
22	Light Emitting Diode	LED
23	photo-luminescence	PL
24	electrochemical impedance spectroscopy	EIS
25	Density Functional Theory	DFT
26	[1,3,5-tris(4-aminophenyl)triazine]	TAPT
27	[1,3,5-tris(4-aminophenyl)benzene]	TAPB
28	solar-to-chemical energy conversion	SCC
29	high resolution transmission electron microscopy	HR-TEM
30	transmission electron microscopy	TEM
31	scanning electron microscopy	SEM
32	water oxidation reaction	WOR
33	oxygen reduction reaction	ORR
34	time-dependent density functional theory	TDDFT
35	excited states	ES
36	electron distribution density	EDD
37	carbon dots	CDs
38	Scanning Transmission Electron Microscopy-Energy Dispersive Spectrometer	STEM-EDS
39	Buchwald-Hartwig	B-H
40	solar to biomass conversion	SBC
41	donor-acceptor	D-A
42	tetraphenylethylene	TPE
43	anthracene	AC
44	Fourier Transform Infrared Spectroscopy	FTIR
45	nuclear magnetic resonance	NMR
46	X-ray photoelectron spectroscopy	XPS
47	ultraviolet visible diffuse reflection spectroscopy	Uv-vis RDS
48	Electron Paramagnetic Resonance	EPR
49	diffuse reflectance fourier transform infrared spectroscopy	DRIFTS
50	High-Angle Annular Dark Field-Scanning Transmission Electron Microscopy	HAADF-STEM

driven of sunlight in principle can supply a cleaner alternative to the present anthraquinone process [164,165]. Currently, COPs have been investigated as photocatalysts for the synthesis of solar fuel because they provide the tunability of synthesis in a large chemical space [166–169]. Table 4 summarizes the recently reported photocatalytic H₂O₂ production by COPs based materials. In 2021, A. I. Cooper group discovered a covalent polymer with linear (DE7) by high throughput experiments, which displayed effective H₂O₂ generation from H₂O and O₂ for about 10 h under visible light driven with the absence of additional sacrificial agents [170]. And designed an initial library containing 60 candidate materials (Fig. 20a-e, h) as baseline. DE7-M was synthesized through microwave heating, which shortened the synthesis time from 2 days to 2 h, and thus enhanced the photoelectric performance. According to the SEM and TEM images, the polymers are mainly consisted of folded sheets (Fig. 20f,g). In addition, the conduction band (CB) with -0.93 V (vs NHE) and valence band (VB) with 1.41 V (vs NHE) for DE7-M have been estimated (Fig. 20i), which exhibit that O₂ reduction and H₂O oxidation are both thermodynamically possible. The mechanism studies

demonstrated that H₂O₂ was produced by gradual reduction of O₂ through light induction.

The efficiency of artificial photosynthesis under environmental conditions is much inferior to the natural solar to biomass conversion (SBC) process. Ouyang and co-workers successfully simulated the NADP-mediated photosynthetic process of green plants via the introduction of redox groups as electron-acceptors in the current covalent polymerization photocatalyst [171]. They synthesized two donor-acceptor (D-A) COPs photocatalysts (TPE-AQ and TPE-AC) through the reaction of the electron donors TPE (tetraphenylethylene) respectively with electron acceptors AQ (anthraquinone) and AC (anthracene) for photocatalytic H₂O₂ preparation (Fig. 21a). The TPE-AQ with D-A structure accelerates photoinduced carriers separation due to AQ powerful electron storage capability, meanwhile, experiments and DFT calculations manifested that each AQ group was able to store one electron under ambient-conditions (Fig. 21b). Fig. 21c displays the energy level distributions of TPE-AQ and TPE-AC, which are used to compare their oxidation and reduction capacities. The photocatalytic H₂O₂ generation rate of TPE-AQ is up to 909 μmol g⁻¹ h⁻¹, which is obviously precede that of a lot of the most studied semiconductors, such as TiO₂, BiVO₄, and 3 times higher in comparison with that of TPE-AC (293 μmol g⁻¹ h⁻¹) (Fig. 21d). Furthermore, the SCC efficiency of TPE-AQ is noticeably as high as 0.26%, which is exceed twice compared with that of the average natural SBC efficiency (0.1%), as well as the highest under ambient-conditions at present. Constructing D-A covalent photocatalyst with electron strong storage properties offers a hopeful way for improving SCC under ambient-conditions. In addition, this method may also be applicable to other SCC systems, such as photocatalytic the splitting of water, CO₂ conversion, and fixing N₂, all of which depend on the same fundamental conversion process of photons to electrons like photocatalytic H₂O₂ generation.

Photocatalytic H₂O₂ generation from the reaction of H₂O and O₂ under visible-light illumination is a prospective method for converting solar into chemical energy. Whereas, lacking particular redox reaction center remains the dominating reason for the low efficiency of photocatalytic H₂O₂ generation. In 2022, Zhong et al. successfully synthesized two novel COPs (AQTEE-COP and NATEE-COP) for efficient photocatalytic H₂O₂ preparation (Fig. 22a), and their compositions and structures were verified by some characterizations, such as Fourier Transform Infrared Spectroscopy (FTIR), PXRD, solid state ¹³C nuclear magnetic resonance (NMR) spectra (Fig. 22b) and X-ray photoelectron spectroscopy (XPS) (Fig. 22c) [172]. It can be seen from Fig. 22d, two COPs both have type I and type IV adsorption-desorption isotherm combinations. The UV-vis DRS (ultraviolet visible diffuse reflection spectroscopy) of AQTEE-COP and NATEE-COP indicated that they both lead to a wide range of visible-light (Fig. 22e). Compared with NATEE-COP, the light absorption of AQTEE-COP with anthraquinone redox center is significantly broadened, which is conducive to improving the efficiency of solar to chemical energy conversion. The electron paramagnetic resonance (EPR) signal of AQTEE-COP is stronger than that of NATEE-COP in the dark or visible light, indicating the unpaired electrons on the AQTEE-COP framework with a higher concentration (Fig. 22f). The above results suggest that AQTEE-COP with a donor-acceptor binary structure is able to improve electron delocalization, thereby promoting the generation of unpaired electrons and facilitating the formation of carriers during photocatalytic reactions. Moreover, AQTEE-COP exhibits an efficient H₂O₂ generation rate of 3204 μmol g⁻¹ h⁻¹ under O₂ with visible-light ($\lambda \geq 400$ nm) illumination and the absence of adding any photosensitizers, organic scavengers or cocatalysts (Fig. 22g, h), which also suggests that H₂O₂ is formed through the O₂ two-electron reduction pathway rather than the H₂O two-electron oxidation pathway. Simultaneously, there was no significant deactivation after the photocatalytic production of H₂O₂ for 5 consecutive runs (Fig. 22i), indicating the excellent stability and reusability. This research offers a new scheme to rationally design the pre-functional COPs-based materials for the conversion of solar to chemical

energy. It should be mentioned that the efficiency of photocatalytic H₂O₂ production from H₂O and O₂ remains relatively low due to the rapid photo-generated charges recombination caused by the inefficient H₂O oxidation. Zhong *et al.* reported an anthraquinone-based COP with dual oxidation centers of triazinyl and alkynyl moieties, which was beneficial to consume photo-generated holes and inhibited electron-hole pairs recombination by enhancing H₂O oxidation reaction. This work supplies new protocols for efficient photocatalytic generation of H₂O₂ from H₂O and O₂ in net water with no additional additives [173].

5. Summary and outlook

The photocatalytic H₂O₂ production from H₂O and O₂ by visible light irradiation is a promising approach to solve the problem of high energy consumption and serious environmental pollution in traditional anthraquinone method. This review based on the principles of photocatalytic H₂O₂ production and oxygen reduction/water oxidation path to improve the photocatalytic H₂O₂ production of various metal-free-based photocatalytic systems, including g-C₃N₄, COFs, CTFs and COPs. The important research results related to this field in recent years have been mainly focused on. Up to now, there is still a big gap between the realization of the goal of industrial application, though rapid development has been made in the research of photocatalytic production of H₂O₂ by metal-free-based materials. The photocatalytic efficiencies of metal-free-based materials are still limited by the narrow range of light absorption and the prone to recombination of photo-generated charges, which have not been completely solved. The low selectivity of the two-electron oxygen reduction path compared with the one-electron or four-electron path, the easy decomposition of H₂O₂ and the high kinetic barrier of water oxidation are still the main reasons for the low efficiency of H₂O₂ production at present. Therefore, the performance of photocatalyst can be further improved from the following aspects:

1) The photocatalytic material with visible light response by the control of structure makes the reduction potential of the conduction band (CB) edge more negative than that of O₂, and the oxidation potential of the valence band (VB) edge more positive than that of H₂O, which are the prerequisite for the photocatalysis of H₂O and O₂ to H₂O₂ in thermodynamics. Therefore, it is the primary problem to obtain a series of metal-free-based photocatalysts with accurate band structure by adjusting the compositions, structures and reaction conditions.

2) Exploring new strategies to extend the light absorption range of metal-free-based photocatalysts. The optimization of the light-harvesting performance of photocatalysts is mainly reflected in the extension of the spectral response range, especially the absorption of visible light or infrared light ($\lambda > 600$ nm), so as to make more effective use of solar energy and slow down the decomposition of H₂O₂ by ultraviolet light.

3) Compared to four-electron O₂ reduction /H₂O oxidation, the two-step one-electron or one-step two-electron path is more dynamic efficient, although it requires a higher redox potential to overcome heat. Therefore, on the basis that catalysts satisfy the thermodynamic O₂ reduction and H₂O oxidation, the identification of the key intermediate species of two-step single electron or one-step two electron O₂ reduction /H₂O oxidation and the corresponding rate control steps are the key scientific problems to preferentially drive the two-step single electron or one-step two electron path.

4) Seeking efficient research methods to extend the life of photo-generated electrons and holes. In the process of photocatalytic reaction, it is necessary to intentionally induce the rapid separation of photo-generated charges to improve the efficiency of photocatalytic H₂O₂ production.

5) Exploring a new way to promote the formation of H₂O₂ and inhibit its decomposition. The efficiency of photocatalytic H₂O₂ production is not satisfactory, although the existing research has made efforts in this aspect. Further researches should focus on the development of more suitable organic semiconductors to further improve the performance of

H₂O₂ production by changing the electronic structure of photocatalytic materials and combining with other modification methods.

6) Increasing the research on the process of H₂O₂ production by water oxidation. Up to now, some progress has been made in the research on H₂O₂ production by two-electron oxygen reduction, while the research on H₂O₂ production by two-electron water oxidation is relatively few. The potential electron transfer pathway is relatively complex in the condition of water and oxygen. In the future, the preparation of H₂O₂ by redox dual path of metal-free materials will be a key research direction. Further studies are needed to improve the performance related to H₂O₂ production by water oxidation.

Although there are many challenges remain and need further efforts to overcome, the metal-free-based photocatalysts still have a promising future for efficient, green and sustainable H₂O₂ generation and will increasingly attract attention from the modern industry owing to their benefits over inorganic metals materials-based catalysts. It is certain that the research of metal-free-based photocatalysts in recent years will arouse the interest of more researchers, promote the exploration of efficient and environmental H₂O₂ production techniques, and promote the development of solar-to-chemical energy conversion. It can be expected that the metal-free-based photocatalysts will have greater application potential in the future photocatalytic H₂O₂ production, and can be extended to other versatile photocatalytic systems, such as H₂ evolution, CO₂ reduction and pollutant degradation and organic photosynthesis. Table 5.

Declaration of Competing Interest

The authors declare that they have no known competing financial interests or personal relationships that could have appeared to influence the work reported in this paper.

Data Availability

Data will be made available on request.

Acknowledgments

This work was financially supported by the National Natural Science Foundation of China (22075286, 22161023 and 42077332), Natural Science Foundation of Jiangxi Province (20224ACB214004, 20232ACB203001 and 20212BAB214029), Department of Education Foundation of Jiangxi Province (GJJ211003, GJJ211042 and GJJ2201641).

References

- [1] R.L. Myers, The 100 Most Important Chemical Compounds, 319, Greenwood Press, London, 2007.
- [2] X. Zhang, P. Ma, C. Wang, L.Y. Gan, X. Chen, P. Zhang, Y. Wang, H. Li, L. Wang, X. Zhou, K. Zheng, Unraveling the dual defect sites in graphite carbon nitride for ultra-high photocatalytic H₂O₂ evolution, Energy Environ. Sci. 15 (2022) 830–842.
- [3] Y. Kuwahara, R. Matsumura, H. Yamashita, Hollow titanosilicate nanospheres encapsulating PdAu alloy nanoparticles as reusable high-performance catalysts for H₂O₂-mediated one-pot oxidation reaction, J. Mater. Chem. A 7 (2019) 7221–7231.
- [4] K.P. Bryliakov, Catalytic asymmetric oxygénations with the environmentally benign oxidants H₂O₂ and O₂, Chem. Rev. 117 (2017) 11406–11459.
- [5] D.B. Miklos, C. Remy, M. Jekel, K.G. Linden, J.E. Drewes, U. Hübner, Evaluation of advanced oxidation processes for water and wastewater treatment-A critical review, Water Res. 139 (2018) 118–131.
- [6] Q. Chen, Development of an anthraquinone process for the production of hydrogen peroxide in a trickle bed reactor-From bench scale to industrial scale, Chem. Eng. Process. 47 (2008) 787–792.
- [7] Z. Chen, D. Yao, C. Chu, S. Mao, Photocatalytic H₂O₂ production Systems: Design strategies and environmental applications, Chem. Eng. J. 451 (2023), 138489.
- [8] X. Wang, X. Zhong, Z. Liu, L. Cheng, Recent progress of chemodynamic therapy-induced combination cancer therapy, Nano Today 35 (2020), 100946.
- [9] J. Tang, T. Zhao, D. Solanki, X. Miao, W. Zhou, S. Hu, Selective hydrogen peroxide conversion tailored by surface, Interface, Device Eng., Joule 5 (2021) 1432–1461.

- [10] S. Fukuzumi, Production of liquid solar fuels and their use in fuel cells, Joule 1 (2017) 689–738.
- [11] Z. Lu, G. Chen, S. Siahrostami, Z. Chen, K. Liu, J. Xie, L. Liao, T. Wu, D. Lin, Y. Liu, T.F. Jaramillo, J.K. Nørskov, Y. Cui, High-efficiency oxygen reduction to hydrogen peroxide catalysed by oxidized carbon materials, Nat. Catal. 1 (2018) 156–162.
- [12] T. Yoshii, Y. Kuwahara, K. Mori, H. Yamashita, Promotional effect of surface plasmon resonance on direct formation of hydrogen peroxide from H₂ and O₂ over Pd/graphene-Au nanorod catalytic system, J. Catal. 394 (2021) 259–265.
- [13] J.M. Campos-Martin, G. Blanco-Brieva, J.L.G. Fierro, Hydrogen peroxide synthesis: an outlook beyond the anthraquinone process, Angew. Chem. Int. Ed. 45 (2006) 6962–6984.
- [14] I.V. Kolesnichenko, P.R. Escamilla, J.A. Michael, V.M. Lynch, D.A.V. Bout, E. V. Anslyn, Hydrogen peroxide production via a redox reaction of N, N'-dimethyl-2,6-diaza-9,10-anthraquinonediium by addition of bisulfite, Chem. Commun. 54 (2018) 11204–11207.
- [15] T. Liu, X. Meng, Y. Wang, X. Liang, Z. Mi, X. Qi, S. Li, W. Wu, E. Min, S. Fu, Integrated process of H₂O₂ generation through anthraquinone hydrogenation-oxidation cycles and the ammoniation of cyclohexanone, Ind. Eng. Chem. Res. 43 (2004) 166–172.
- [16] Y. Wang, G.I.N. Waterhouse, L. Shang, T. Zhang, Electrocatalytic oxygen reduction to hydrogen peroxide: from homogeneous to heterogeneous electrocatalysis, Adv. Energy Mater. 11 (2021) 2003323.
- [17] S. Lu, L. Wang, Y. Wang, Z. Mi, Kinetic model of gas-liquid-liquid reactive extraction for production of hydrogen peroxide, Chem. Eng. Technol. 34 (2011) 823–830.
- [18] A. Pashkova, K. Svajda, R. Dittmeyer, Direct synthesis of hydrogen peroxide in a catalytic membrane contactor, Chem. Eng. J. 139 (2008) 165–171.
- [19] E. Santacesaria, M. Di Serio, A. Russo, U. Leone, R. Velotti, Kinetic and catalytic aspects in the hydrogen peroxide production via anthraquinone, Chem. Eng. Sci. 54 (1999) 2799–2806.
- [20] K. Brudzynski, D. Miotti, L. Kim, C. Sjaarda, L. Maldonado-Alvarez, H. Fuká, Active macromolecules of honey form colloidal particles essential for honey antibacterial activity and hydrogen peroxide production, Sci. Rep. 7 (2017) 7637.
- [21] Y. Kondo, Y. Kuwahara, K. Mori, H. Yamashita, Design of metal-organic framework catalysts for photocatalytic hydrogen peroxide production, Chem 8 (2022) 2924–2938.
- [22] H. Zhang, M. Liu, Q. Miao, P. Wu, C. Liu, W. Jiang, Sustainable H₂O₂ photosynthesis by sunlight and air, Chem. Eng. J. 455 (2023), 140649.
- [23] Y. Isaka, Y. Kawase, Y. Kuwahara, K. Mori, H. Yamashita, Two-phase system utilizing hydrophobic metal-organic frameworks (MOFs) for photocatalytic synthesis of hydrogen peroxide, Angew. Chem. Int. Ed. 58 (2019) 5402–5406.
- [24] Y. Shiraishi, M. Matsumoto, S. Ichikawa, S. Tanaka, T. Hirai, Polythiophene-doped resorcinol-formaldehyde resin photocatalysts for solar-to-hydrogen peroxide energy conversion, J. Am. Chem. Soc. 143 (2021) 12590–12599.
- [25] C. Liang, X.W. Wang, W. Liu, H.Y. Liu, D.W. Huang, Y.Z. Zhang, K.H. Zhang, L.S. Jiang, Y.Y. Jia, C.G. Niu, Functionalized graphitic carbon nitride based catalysts in solar-to-chemical conversion for hydrogen peroxide production, Chem. Eng. J. 466 (2023), 142931.
- [26] Y. Sun, L. Han, P. Strasser, A comparative perspective of electrochemical and photochemical approaches for catalytic H₂O₂ production, Chem. Soc. Rev. 49 (2020) 6605–6631.
- [27] H. Hou, X. Zeng, X. Zhang, Production of hydrogen peroxide by photocatalytic processes, Angew. Chem. Int. Ed. 59 (2020) 17356–17376.
- [28] Y. Kondo, K. Hino, Y. Kuwahara, K. Mori, H. Yamashita, Photosynthesis of hydrogen peroxide from dioxygen and water using aluminium-based metal-organic framework assembled with porphyrin- and pyrene-based linkers, J. Mater. Chem. A 11 (2023) 9530–9537.
- [29] G. Moon, W. Kim, A.D. Bokare, N. Sung, W. Choi, Solar production of H₂O₂ on reduced graphene oxide-TiO₂ hybrid photocatalysts consisting of earth-abundant elements only, Energy Environ. Sci. 7 (2014) 4023–4028.
- [30] H. Hirakawa, S. Shiota, Y. Shiraishi, H. Sakamoto, S. Ichikawa, T. Hirai, Au nanoparticles supported on BiVO₄: Effective inorganic photocatalysts for H₂O₂ production from water and O₂ under visible light, ACS Catal. 6 (2016) 4976–4982.
- [31] H. Song, L. Wei, C. Chen, C. Wen, F. Han, Photocatalytic production of H₂O₂ and its in situ utilization over atomic-scale Au modified MoS₂ nanosheets, J. Catal. 376 (2019) 198–208.
- [32] C. Liu, T. Bao, L. Yuan, C. Zhang, J. Wang, J. Wan, C. Yu, Semiconducting MOF@ZnS Heterostructures for photocatalytic hydrogen peroxide production: heterojunction coverage matters, Adv. Funct. Mater. 32 (2022) 211404.
- [33] B. Chong, H. Li, B. Xu, G. Yang, Hollow double-shell stacked CdS@ZnIn₂S₄ photocatalyst incorporating spatially separated dual cocatalysts for the enhanced photocatalytic hydrogen evolution and hydrogen peroxide production, Catal. Today 405–406 (2022) 227–234.
- [34] S. Kumar, V.R. Battula, N. Sharma, S. Samanta, B. Rawat, K. Kailasam, A metal-free heptazine-porphyrin based porous polymeric network as an artificial leaf for carbon-free solar fuels, J. Mater. Chem. A 10 (2022) 14568–14575.
- [35] Z. Wei, M. Liu, Z. Zhang, W. Yao, H. Tan, Y. Zhu, Efficient visible-light-driven selective oxygen reduction to hydrogen peroxide by oxygen-enriched graphitic carbon nitride polymers, Energy Environ. Sci. 11 (2018) 2581–2589.
- [36] X. Yu, B. Viengkeo, Q. He, X. Zhao, Q. Huang, P. Li, W. Huang, Y. Li, Electronic tuning of covalent triazine framework nanoshells for highly efficient photocatalytic H₂O₂ production, Adv. Sustain. Syst. 5 (2021) 2100184.
- [37] C.T.J. Ferguson, K.A.I. Zhang, Classical polymers as highly tunable and designable heterogeneous photocatalysts, ACS Catal. 11 (2021) 9547–9560.
- [38] Q. Tian, L. Jing, S. Ye, J. Liu, R. Chen, C.A.H. Price, F. Fan, J. Liu, Nanospacial charge modulation of monodispersed polymeric microsphere photocatalysts for exceptional hydrogen peroxide production, Small 17 (2021) 2103224.
- [39] Y. Wang, A. Vogel, M. Sachs, R.S. Sprick, L. Wilbraham, S.J.A. Moniz, R. Godin, M.A. Zwijnenburg, J.R. Durrant, A.I. Cooper, J. Tang, Current understanding and challenges of solar-driven hydrogen generation using polymeric photocatalysts, Nat. Energy 4 (2019) 746–760.
- [40] C. Zhao, Z. Chen, R. Shi, X. Yang, T. Zhang, Recent advances in conjugated polymers for visible-light-driven water splitting, Adv. Mater. 32 (2020) 1907296.
- [41] L. Yuan, C. Zhang, J. Wang, C. Liu, C. Yu, Mesoporous resin nanobowls with optimized donor-acceptor conjugation for highly efficient photocatalytic hydrogen peroxide production, Nano Res. 14 (2021) 3267–3273.
- [42] Y. Yang, Z. Zeng, G. Huang, R. Xiao, C. Zhang, C. Zhou, W. Xiong, W. Wang, M. Cheng, W. Xue, H. Guo, X. Tang, D. He, Ti₃C₂ mxene/porous g-C₃N₄ interfacial schottky junction for boosting spatial charge separation in photocatalytic H₂O₂ production, Appl. Catal. B: Environ. 258 (2019), 117956.
- [43] Y. Shiraishi, S. Kanazawa, Y. Kofuji, H. Sakamoto, S. Ichikawa, S. Tanaka, T. Hirai, Sunlight-driven hydrogen peroxide production from water and molecular oxygen by metal-free photocatalysts, Angew. Chem. Int. Ed. 53 (2014) 13454–13459.
- [44] J. Kosco, S. Gonzalez-Carrero, C.T. Howells, T. Fei, Y. Dong, R. Sougrat, G. T. Harrison, Y. Firdaus, R. Sheelamanthula, B. Purushothaman, F. Moruzzi, W. Xu, L. Zhao, A. Basu, S. De Wolf, T.D. Anthopoulos, J.R. Durrant, I. McCulloch, Generation of long-lived charges in organic semiconductor heterojunction nanoparticles for efficient photocatalytic hydrogen evolution, Nat. Energy 7 (2022) 340–351.
- [45] Y. Kofuji, S. Ohkita, Y. Shiraishi, H. Sakamoto, S. Tanaka, S. Ichikawa, T. Hirai, Graphitic carbon nitride doped with biphenyl diimide: efficient photocatalyst for hydrogen peroxide production from water and molecular oxygen by sunlight, ACS Catal. 6 (2016) 7021–7029.
- [46] L. Zhai, Z. Xie, C.X. Cui, X. Yang, Q. Xu, X. Ke, M. Liu, L.B. Qu, X. Chen, L. Mi, Constructing synergistic triazine and acetylene cores in fully conjugated covalent organic frameworks for cascade photocatalytic H₂O₂ production, Chem. Mater. 34 (2022) 5232–5240.
- [47] Y. Zhao, P. Zhang, Z. Yang, L. Li, J. Gao, S. Chen, T. Xie, C. Diao, S. Xi, B. Xiao, C. Hu, W. Choi, Mechanistic analysis of multiple processes controlling solar-driven H₂O₂ synthesis using engineered polymeric carbon nitride, Nat. Commun. 12 (2021) 3701.
- [48] H. Zhong, R. Sa, H. Lv, S. Yang, D. Yuan, X. Wang, R. Wang, Covalent organic framework Hosting Metalloporphyrin-Based Carbon Dots for Visible-Light-Driven Selective CO₂ Reduction, Adv. Funct. Mater. 30 (2020) 2002654.
- [49] Z. Teng, W. Cai, S. Liu, C. Wang, Q. Zhang, S. Chenliang, T. Ohno, Bandgap engineering of polymetric carbon nitride copolymerized by 2,5,8-triamino-tri-siazine (melem) and barbituric acid for efficient nonsacrificial photocatalytic H₂O₂ production, Appl. Catal. B: Environ. 271 (2020), 118917.
- [50] R. Wang, K. Pan, D. Han, J. Jiang, C. Xiang, Z. Huang, L. Zhang, X. Xiang, Solar-driven H₂O₂ generation from H₂O and O₂ using earth-abundant mixed-metal oxide@carbon nitride photocatalysts, ChemSusChem 9 (2016) 2470–2479.
- [51] C. Xia, H. Wang, J.K. Kim, J. Wang, Rational design of metal oxide-based heterostructure for efficient photocatalytic and photoelectrochemical systems, Adv. Funct. Mater. 31 (2021) 2008247.
- [52] H. Zhong, Z. Hong, C. Yang, L. Li, Y. Xu, X. Wang, R. Wang, A covalent triazine-based framework consisting of donor-acceptor dyads for visible-light-driven photocatalytic CO₂ reduction, ChemSusChem 12 (2019) 4493–4499.
- [53] X. Xu, W. Huang, X. Li, Y. Sui, W. Chen, Y. Li, H. Ye, C. Pan, H. Zhong, M. Wen, Triphenylamine-based covalent triazine framework @ carbon nanotube complex: efficient photogenerated charges migration for metal free photocatalytic Cr(VI) reduction, J. Environ. Chem. Eng. 11 (2023), 109331.
- [54] H. Zhong, C. Yang, L. Fan, Z. Fu, X. Yang, X. Wang, R. Wang, Dyadic promotion of photocatalytic aerobic oxidation via the Mott-Schottky effect enabled by nitrogen-doped carbon from imidazolium-based ionic polymer, Energy Environ. Sci. 12 (2019) 418–426.
- [55] S. Yang, R. Sa, H. Zhong, H. Lv, D. Yuan, R. Wang, Microenvironments enabled by covalent organic framework linkages for modulating active metal species in photocatalytic CO₂ reduction, Adv. Funct. Mater. 32 (2022) 2110694.
- [56] H. Cheng, J. Cheng, L. Wang, H. Xu, Reaction pathways toward sustainable photosynthesis of hydrogen peroxide by polymer photocatalysts, Chem. Mater. 34 (2022) 4259–4273.
- [57] S.Y. Park, H. Abroshan, X. Shi, H.S. Jung, S. Siahrostami, X. Zheng, CaSnO₃: an electrocatalyst for two-electron water oxidation reaction to form H₂O₂, ACS Energy Lett. 4 (2019) 352–357.
- [58] J.H. Baek, T.M. Gill, H. Abroshan, S. Park, X. Shi, J. Nørskov, H.S. Jung, S. Siahrostami, X. Zheng, Selective and efficient Gd-doped BiVO₄ photoanode for two-electron water oxidation to H₂O₂, ACS Energy Lett. 4 (2019) 720–728.
- [59] X. Chen, W. Zhang, L. Zhang, L. Feng, C. Zhang, J. Jiang, T. Yan, H. Wang, Sacrificial agent-free photocatalytic H₂O₂ evolution via two-electron oxygen reduction using a ternary α-Fe₂O₃/CQD@g-C₃N₄ photocatalyst with broadspectrum response, J. Mater. Chem. A 8 (2020) 18816–18825.
- [60] J. Xiong, X. Li, J. Huang, X. Gao, Z. Chen, J. Liu, H. Li, B. Kang, W. Yao, Y. Zhu, CN/rGO@BPQDs high-low junctions with stretching spatial charge separation ability for photocatalytic degradation and H₂O₂ production, Appl. Catal. B: Environ. 266 (2020), 118602.
- [61] X. Zeng, Y. Liu, X. Hu, X. Zhang, Photoredox catalysis over semiconductors for light-driven hydrogen peroxide production, Green Chem. 23 (2021) 1466–1494.
- [62] K. Li, Q. Ge, Y. Liu, L. Wang, K. Gong, J. Liu, L. Xie, W. Wang, X. Ruana, L. Zhang, Highly efficient photocatalytic H₂O₂ production in microdroplets: Accelerated

- charge separation at interfaces, *Energy Environ. Sci.* 16 (2023) 1135–1145.
- [63] S. Fukuzumi, Y.M. Lee, W. Nam, Solar-driven production of hydrogen peroxide from water and dioxygen, *Chem. -Eur. J.* 24 (2018) 5016.
- [64] F. Wang, Q. Li, D. Xu, Recent progress in semiconductor based nanocomposite photocatalysts for solar-to-chemical energy conversion, *Adv. Energy Mater.* 7 (2017) 1700529.
- [65] T. Liu, Z. Pan, J.J.M. Vequizo, K. Kato, B. Wu, A. Yamakata, K. Katayama, B. Chen, C. Chu, K. Domen, Overall photosynthesis of H₂O₂ by an inorganic semiconductor, *Nat. Commun.* 13 (2022) 1034.
- [66] H. Tan, P. Zhou, M. Liu, Q. Zhang, F. Liu, H. Guo, Y. Zhou, Y. Chen, L. Zeng, L. Gu, Z. Zheng, M. Tong, S. Guo, Photocatalysis of water into hydrogen peroxide over an atomic Ga-N₅ site, *Nat. Synth.* 2 (2023) 557–563.
- [67] C. Feng, Z.P. Wu, K.W. Huang, J. Ye, H. Zhang, Surface modification of 2D photocatalysts for solar energy conversion, *Adv. Mater.* 34 (2022) 2200180.
- [68] X. Zhang, J. Yu, W. Macyk, S. Wageh, A.A. Al-Ghamdi, L. Wang, C₃N₄/PDA S-scheme heterojunction with enhanced photocatalytic H₂O₂ production performance and its mechanism, *Adv. Sustain. Syst.* 7 (2023) 2200113.
- [69] L. Xue, H. Sun, Q. Wu, W. Yao, P-doped melon-carbon nitride for efficient photocatalytic H₂O₂ production, *J. Colloid Interface Sci.* 615 (2022) 87–94.
- [70] Y. Shiraishi, Y. Kofuji, H. Sakamoto, S. Tanaka, S. Ichikawa, T. Hirai, Effects of surface defects on photocatalytic H₂O₂ production by mesoporous graphitic carbon nitride under visible light irradiation, *ACS Catal.* 5 (2015) 3058–3066.
- [71] Z. Yu, K. Yang, C. Yu, K. Lu, W. Huang, L. Xu, L. Zou, S. Wang, Z. Chen, J. Hu, Y. Hou, Y. Zhu, Steering unit cell dipole and internal electric field by highly dispersed Er atoms embedded into NiO for efficient CO₂ photoreduction, *Adv. Funct. Mater.* 32 (2022) 2111999.
- [72] C. Zhu, M. Zhu, Y. Sun, Y. Zhou, J. Gao, H. Huang, Y. Liu, Z. Kang, Carbon-supported oxygen vacancy-rich Co₃O₄ for robust photocatalytic H₂O₂ production via coupled water oxidation and oxygen reduction reaction, *ACS Appl. Energy Mater.* 2 (2019) 8737–8746.
- [73] F. Xue, Y. Si, M. Wang, M. Liu, L. Guo, Toward efficient photocatalytic pure water splitting for simultaneous H₂ and H₂O₂ production, *Nano Energy* 62 (2019) 823–831.
- [74] W. Wang, W. Zhang, Y. Cai, Q. Wang, J. Deng, J. Chen, Z. Jiang, Y. Zhang, C. Yu, Introducing B-N unit boosts photocatalytic H₂O₂ production on metal-free g-C₃N₄ nanosheets, *Nano Res* 16 (2023) 2177–2184.
- [75] H. Song, L. Wei, C. Chen, C. Wen, F. Han, Photocatalytic production of H₂O₂ and its in situ utilization over atomic-scale Au modified MoS₂ nanosheets, *J. Catal.* 376 (2019) 198–208.
- [76] F. Kuttasser, A. Sebastian, S. Mathew, H. Tachibana, H. Inoue, Promotive effect of bicarbonate ion on two-electron water oxidation to form H₂O₂ catalyzed by aluminum porphyrins, *ChemSusChem* 12 (2019) 1939–1948.
- [77] Q. Zhang, J. Pan, Z. Zhuo, M. Xiang, Q. Yan, Abrasion behavior of TiO₂ catalyzing H₂O₂ to synergistically remove single crystal 6H-SiC under ultraviolet irradiation, *Surf. Interfaces* 38 (2023), 102781.
- [78] L. Zou, R. Sa, H. Zhong, H. Lv, X. Wang, R. Wang, Photoelectron transfer mediated by the interfacial electron effects for boosting visible-light-driven CO₂ reduction, *ACS Catal.* 12 (2022) 3550–3557.
- [79] P. Ma, X. Zhang, C. Wang, Z. Wang, K. Wang, Y. Feng, J. Wang, Y. Zhai, J. Deng, L. Wang, K. Zheng, Band alignment of homojunction by anchoring CN quantum dots on g-C₃N₄ (0D/2D) enhance photocatalytic hydrogen peroxide evolution, *Appl. Catal. B: Environ.* 300 (2022), 120736.
- [80] X. Wang, K. Maeda, A. Thomas, K. Takanabe, G. Xin, J.M. Carlsson, K. Domen, M. Antonietti, A metal-free polymeric photocatalyst for hydrogen production from water under visible light, *Nat. Mater.* 8 (2009) 76–82.
- [81] S. Cao, J. Yu, g-C₃N₄-based photocatalysts for hydrogen generation, *J. Phys. Chem. Lett.* 5 (2014) 2101–2107.
- [82] W. Liu, R. Xu, W. Pan, C. Li, N. Huang, Y. Huang, L. Ye, Solar-to-H₂O₂ energy conversion by the photothermal effect of a polymeric photocatalyst via a two-channel pathway, *ChemSusChem* 16 (2023), e202300015.
- [83] Y. Shiraishi, S. Kanazawa, Y. Sugano, D. Tsukamoto, H. Sakamoto, S. Ichikawa, T. Hirai, Highly selective production of hydrogen peroxide on graphitic carbon nitride (g-C₃N₄) photocatalyst activated by visible light, *ACS Catal.* 4 (2014) 774–780.
- [84] Y. Kofuji, S. Ohkita, Y. Shiraishi, H. Sakamoto, S. Tanaka, S. Ichikawa, T. Hirai, Graphitic carbon nitride doped with biphenyl diimide: efficient photocatalyst for hydrogen peroxide production from water and molecular oxygen by sunlight, *ACS Catal.* 6 (2016) 7021–7029.
- [85] Y. Shiraishi, S. Kanazawa, Y. Kofuji, H. Sakamoto, S. Ichikawa, S. Tanaka, T. Hirai, Sunlight-driven hydrogen peroxide production from water and molecular oxygen by metal-free photocatalysts, *Angew. Chem. Int. Ed.* 53 (2014) 13454–13459.
- [86] Y. Kofuji, S. Ohkita, Y. Shiraishi, H. Sakamoto, S. Ichikawa, S. Tanaka, T. Hirai, Mellitic triimide-doped carbon nitride as sunlight-driven photocatalysts for hydrogen peroxide production, *ACS Sustain. Chem. Eng.* 5 (2017) 6478–6485.
- [87] H. Kim, S. Gim, T.H. Jeon, H. Kim, W. Choi, Distorted carbon nitride structure with substituted benzene moieties for enhanced visible light photocatalytic activities, *ACS Appl. Mater. Interfaces* 9 (2017) 40360–40368.
- [88] J. Xiao, Q. Liu, M. Song, X. Li, Q. Li, J.K. Shang, Directing photocatalytic pathway to exceedingly high antibacterial activity in water by functionalizing holey ultrathin nanosheets of graphitic carbon nitride, *Water Res* 198 (2021), 117125.
- [89] X. Zeng, Y. Liu, Y. Xia, M.H. Uddin, D. Xia, D.T. McCarthy, A. Deletic, J. Yu, X. Zhang, Cooperatively modulating reactive oxygen species generation and bacteria-photocatalyst contact over graphitic carbon nitride by polyethylenimine for rapid water disinfection, *Appl. Catal. B: Environ.* 274 (2020), 119095.
- [90] Z. Teng, N. Yang, H. Lv, S. Wang, M. Hu, C. Wang, D. Wang, G. Wang, Edge functionalized g-C₃N₄ nanosheets as a highly efficient metal-free photocatalyst for safe drinking water, *Chem* 5 (2019) 664–680.
- [91] H. Kim, Y. Choi, S. Hu, W. Choi, J.H. Kim, Photocatalytic hydrogen peroxide production by anthraquinone-augmented polymeric carbon nitride, *Appl. Catal. B: Environ.* 229 (2018) 121–129.
- [92] W. Liu, R. Xu, Y. Wang, N. Huang, T. Shimada, L. Ye, AQ-coupled few-layered g-C₃N₄ nanoplates obtained by one-step mechanochemical treatment for efficient visible-light photocatalytic H₂O₂ production, *Int. J. Hydrog. Energy* 47 (2022), 16005e16013.
- [93] C. Chu, Q. Zhu, Z. Pan, S. Gupta, D. Huang, Y. Du, S. Weon, Y. Wu, C. Muhich, E. Stavitski, K. Domen, J.H. Kim, Spatially separating redox centers on 2D carbon nitride with cobalt single atom for photocatalytic H₂O₂ production, *PNAS* 117 (2020) 6376–6382.
- [94] X. Qu, S. Hu, P. Li, Z. Li, H. Wang, H. Ma, W. Li, The effect of embedding N vacancies into g-C₃N₄ on the photocatalytic H₂O₂ production ability via H₂ plasma treatment, *Diam. Relat. Mater.* 86 (2018) 159–166.
- [95] X. Li, J. Zhang, F. Zhou, H. Zhang, J. Bai, Y. Wang, H. Wang, Preparation of N-vacancy-doped g-C₃N₄ with outstanding photocatalytic H₂O₂ production ability by dielectric barrier discharge plasma treatment, *Chin. J. Catal.* 39 (2018) 1090–1098.
- [96] L. Shi, L. Yang, W. Zhou, Y. Liu, L. Yin, X. Hai, H. Song, J. Ye, Photoassisted construction of holey defective g-C₃N₄ photocatalysts for efficient visible-light-driven H₂O₂ production, *Small* 14 (2018) 1703142.
- [97] S. Li, G. Dong, R. Hailli, L. Yang, Y. Li, F. Wang, Y. Zeng, C. Wang, Effective photocatalytic H₂O₂ production under visible light irradiation at g-C₃N₄ modulated by carbon vacancies, *Appl. Catal. B: Environ.* 190 (2016) 26–35.
- [98] S. Wu, H. Yu, S. Chen, X. Quan, Enhanced photocatalytic H₂O₂ production over carbon nitride by doping and defect engineering, *ACS Catal.* 10 (2020) 14380–14389.
- [99] L. Chen, C. Chen, Z. Yang, S. Li, C. Chu, B. Chen, Simultaneously tuning band structure and oxygen reduction pathway toward high-efficient photocatalytic hydrogen peroxide production using cyano-rich graphitic carbon nitride, *Adv. Funct. Mater.* 31 (2021) 2105731.
- [100] P. Zhang, Y. Tong, Y. Liu, J.J.M. Vequizo, H. Sun, C. Yang, A. Yamakata, F. Fan, W. Lin, X. Wang, W. Choi, Heteroatom dopants promote two-electron O₂ reduction for photocatalytic production of H₂O₂ on polymeric carbon nitride, *Angew. Chem. Int. Ed.* 59 (2020) 16209–16217.
- [101] P. Zhang, D. Sun, A. Cho, S. Weon, S. Lee, J. Lee, J.W. Han, D.P. Kim, W. Choi, Modified carbon nitride nanozyme as bifunctional glucose oxidase-peroxidase for metal-free bioinspired cascade photocatalysis, *Nat. Commun.* 10 (2019) 940.
- [102] Z. Li, N. Xiong, G. Gu, Fabrication of a full-spectrum-response Cu₂(OH)₂CO₃/g-C₃N₄ heterojunction catalyst with outstanding photocatalytic H₂O₂ production performance via a self-sacrificial method, *Dalton Trans.* 48 (2019) 182–189.
- [103] X. Hu, X. Zeng, Y. Liu, J. Lu, S. Yuan, Y. Yin, J. Hu, D.T. McCarthy, X. Zhang, Nano-layer based 1T-rich MoS₂/g-C₃N₄ co-catalyst system for enhanced photocatalytic and photoelectrochemical activity, *Appl. Catal. B: Environ.* 268 (2020), 118466.
- [104] G.H. Moon, M. Fujitsuka, S. Kim, T. Majima, X. Wang, W. Choi, Eco-friendly photochemical production of H₂O₂ through O₂ reduction over carbon nitride frameworks incorporated with multiple heteroelements, *ACS Catal.* 7 (2017) 2886–2895.
- [105] S. Kim, G.H. Moon, H. Kim, Y. Mun, P. Zhang, J. Lee, W. Choi, Selective charge transfer to dioxygen on KPF6-modified carbon nitride for photocatalytic synthesis of H₂O₂ under visible light, *J. Catal.* 357 (2018) 51–58.
- [106] P. Zhang, Y. Liu, J.J.M. Vequizo, H.W. Sun, C. Yang, A. Yamakata, F.T. Fan, W. Lin, X.C. Wang, W. Choi, Heteroatom dopants promote two-electron O₂ reduction for photocatalytic production of H₂O₂ on polymeric carbon nitride, *Angew. Chem. Int. Ed.* 59 (2020) 16209–16217.
- [107] J. Zhang, C. Yu, J. Lang, Y. Zhou, B. Zhou, Y.H. Hu, M. Long, Modulation of lewis acidic-basic sites for efficient photocatalytic H₂O₂ production over potassium intercalated tri-s-triazine materials, *Appl. Catal. B: Environ.* 277 (2020), 119225.
- [108] S. Hu, X. Qu, P. Li, F. Wang, Q. Li, L. Song, Y. Zhao, X. Kang, Photocatalytic oxygen reduction to hydrogen peroxide over copper doped graphitic carbon nitride hollow microsphere: The effect of Cu(I)-N active sites, *Chem. Eng. J.* 334 (2018) 410–418.
- [109] S. Samanta, R. Yadav, A. Kumar, A.K. Sinha, R. Srivastava, Surface modified C, O co-doped polymeric g-C₃N₄ as an efficient photocatalyst for visible light assisted CO₂ reduction and H₂O₂ production, *Appl. Catal. B: Environ.* 259 (2019), 118054.
- [110] X. Chang, J. Yang, D. Han, B. Zhang, X. Xiang, J. He, Enhancing light-driven production of hydrogen peroxide by anchoring Au onto C₃N₄ catalysts, *Catalysts* 8 (2018) 147.
- [111] Y. Peng, L. Wang, Y. Liu, H. Chen, J. Lei, J. Zhang, Visible-light-driven photocatalytic H₂O₂ production on g-C₃N₄ loaded with CoP as a noble metal free cocatalyst, *Eur. J. Inorg. Chem.* 2017 (2017) 4797–4802.
- [112] Z. Teng, W. Cai, W. Sim, Q. Zhang, C. Wang, C. Su, T. Ohno, Photoexcited single metal atom catalysts for heterogeneous photocatalytic H₂O₂ production: Pragmatic guidelines for predicting charge separation, *Appl. Catal. B: Environ.* 282 (2021), 119589.
- [113] L. Zhou, J. Feng, B. Qiu, Y. Zhou, J. Lei, M. Xing, L. Wang, Y. Zhou, Y. Liu, J. Zhang, Ultrathin g-C₃N₄ nanosheet with hierarchical pores and desirable energy band for highly efficient H₂O₂ production, *Appl. Catal. B: Environ.* 267 (2020), 118396.
- [114] H. Ou, P. Yang, L. Lin, M. Anpo, X. Wang, Carbon nitride aerogels for the photoredox conversion of water, *Angew. Chem. Int. Ed.* 56 (2017) 10905–10910.

- [115] S. Zhao, T. Guo, X. Li, T. Xu, B. Yang, X. Zhao, Carbon nanotubes covalent combined with graphitic carbon nitride for photocatalytic hydrogen peroxide production under visible light, *Appl. Catal. B: Environ.* 224 (2018) 725–732.
- [116] R. Wang, X. Zhang, F. Li, D. Cao, M. Pu, D. Han, J. Yang, X. Xiang, Energy-level dependent H₂O₂ production on metal-free, carbon-content tunable carbon nitride photocatalysts, *J. Energy Chem.* 27 (2018) 343–350.
- [117] Y. Yang, Z. Zeng, G. Zeng, D. Huang, R. Xiao, C. Zhang, C. Zhou, W. Xiong, W. Wang, M. Cheng, Ti₃C₂ MXene/porous g-C₃N₄ interfacial schottky junction for boosting spatial charge separation in photocatalytic H₂O₂ production, *Appl. Catal. B: Environ.* 258 (2019), 117956.
- [118] J. Cai, J. Huang, S. Wang, J. Iocozzia, Z. Sun, J. Sun, Y. Yang, Y. Lai, Z. Lin, Crafting mussel-inspired metal nanoparticle-decorated ultrathin graphitic carbon nitride for the degradation of chemical pollutants and production of chemical resources, *Adv. Mater.* 31 (2019) 1806314.
- [119] Y. Kofuji, Y. Isobe, Y. Shiraishi, H. Sakamoto, S. Tanaka, S. Ichikawa, T. Hirai, Carbon nitride-aromatic diimide-graphene nanohybrids: Metal free photocatalysts for solar-to-hydrogen peroxide energy conversion with 0.2% efficiency, *J. Am. Chem. Soc.* 138 (2016) 10019–10025.
- [120] R. Liu, K.T. Tan, Y. Gong, Y. Chen, Z. Li, S. Xie, T. He, Z. Lu, H. Yanga, D. Jiang, Covalent organic frameworks: an ideal platform for designing ordered materials and advanced applications, *Chem. Soc. Rev.* 50 (2021) 120–242.
- [121] K. Geng, T. He, R. Liu, K.T. Tan, Z. Li, S. Tao, Y. Gong, Q. Jiang, D. Jiang, Covalent organic frameworks: design, synthesis, and functions, *Chem. Rev.* 120 (2020) 8814–8933.
- [122] A.P. Cote, A.J. Benin, N.W. Ockwig, M. Ó Keeffe, A.J. Matzger, O.M. Yaghi, Porous, crystalline, covalent organic frameworks, *Science* 310 (2005) 1166–1170.
- [123] P. Das, G. Chakraborty, J. Roessner, S. Vogl, J. Rabeh, A. Thomas, Integrating bifunctionality and chemical stability in covalent organic frameworks via one-pot bifunctional reactions for solar-driven H₂O₂ production, *J. Am. Chem. Soc.* 145 (2023) 2975–2984.
- [124] C. Shao, Q. He, M. Zhang, L. Jia, Y. Ji, Y. Hu, Y. Li, W. Huang, Y. Li, A covalent organic framework inspired by C₃N₄ for photosynthesis of hydrogen peroxide with high quantum efficiency, *Chin. J. Catal.* 46 (2023) 28–35.
- [125] Z. Zhou, M. Sun, Y. Zhu, P. Li, Y. Zhang, M. Wang, Y. Shen, A thioether-decorated triazine-based covalent organic framework towards overall H₂O₂ photosynthesis without sacrificial agents, *Appl. Catal. B: Environ.* 334 (2023), 122862.
- [126] Y. Luo, B. Zhang, C. Liu, D. Xia, X. Ou, Y. Cai, Y. Zhou, J. Jiang, B. Han, Sulfone-modified covalent organic frameworks enabling efficient photocatalytic hydrogen peroxide generation via one-step two-electron O₂ reduction, *Angew. Chem. Int. Ed.* 62 (2023), e202305355.
- [127] X. Zhang, J. Zhang, J. Miao, X. Wen, C. Chen, B. Zhou, M. Long, Keto-enamine-based covalent organic framework with controllable anthraquinone moieties for superior H₂O₂ photosynthesis from O₂ and water, *Chem. Eng. J.* 466 (2023), 143085.
- [128] Q. Zhi, W. Liu, R. Jiang, X. Zhan, Y. Jin, X. Chen, X. Yang, K. Wang, W. Cao, D. Qi, J. Jiang, Piperazine-linked metalphthalocyanine frameworks for highly efficient visible-light-driven H₂O₂ photosynthesis, *J. Am. Chem. Soc.* 144 (2022) 21328–21336.
- [129] X. Di, X. Lv, H. Wang, F. Chen, S. Wang, G. Zheng, B. Wang, Q. Han, Enhanced pre-sensitization in metal-free covalent organic frameworks promoting hydrogen peroxide photosynthesis, *Chem. Eng. J.* 455 (2023), 140124.
- [130] M. Wu, Z. Shan, J. Wang, T. Liu, G. Zhang, Three-dimensional covalent organic framework with ty topology for enhanced photocatalytic hydrogen peroxide production, *Chem. Eng. J.* 454 (2023), 140121.
- [131] Y. Yang, J. Kang, Y. Li, J. Liang, J. Liang, D. Chen, J. He, Y. Chen, J. Wang, Enhanced photocatalytic hydrogen peroxide production activity of imine-linked covalent organic frameworks via modification with functional groups, *N. J. Chem.* 46 (2022) 21605–21614.
- [132] M. Deng, J. Sun, A. Laemont, C. Liu, L. Wang, L. Bourd, J. Chakraborty, K. V. Hecke, R. Morent, N.D. Geyer, K. Leus, H. Chen, P.V.D. Voort, Extending the π-conjugation system of covalent organic frameworks for more efficient photocatalytic H₂O₂ production, *Green. Chem.* 25 (2023) 3069–3076.
- [133] J. Sun, H.S. Jena, C. Krishnaraj, K.S. Rawat, S. Abednatanz, J. Chakraborty, A. Laemont, W. Liu, H. Chen, Y.Y. Liu, K. Leus, H. Vrielinck, V.V. Speybroeck, P.V. D. Voort, Pyrene-based covalent organic frameworks for photocatalytic hydrogen peroxide production, *Angew. Chem. Int. Ed.* 62 (2023), e202216719.
- [134] T. Yang, Y. Chen, Y. Wang, X. Peng, A. Kong, Weakly hydrophilic imine-linked covalent benzene-acetylene frameworks for photocatalytic H₂O₂ production in the two-phase system, *ACS Appl. Mater. Interfaces* 15 (2023) 8066–8075.
- [135] W. Zhao, P. Yan, B. Li, M. Bahri, L. Liu, X. Zhou, R. Clowes, N.D. Browning, Y. Wu, J.W. Ward, A.I. Cooper, Accelerated synthesis and discovery of covalent organic framework photocatalysts for hydrogen peroxide production, *J. Am. Chem. Soc.* 144 (2022) 9902–9909.
- [136] C. Krishnaraj, H.S. Jena, L. Bourda, A. Laemont, P. Pachfule, J. Roessner, C. V. Chandran, S. Borgmans, S.M.J. Rogge, K. Leus, C.V. Stevens, J.A. Martens, V. V. Speybroeck, E. Breynaert, A. Thomas, P.V.D. Voort, Strongly reducing (diarylamino)benzene-based covalent organic framework for metal-free visible light photocatalytic H₂O₂ generation, *J. Am. Chem. Soc.* 142 (2020) 20107–20116.
- [137] L. Zhai, Z. Xie, C.X. Cui, X. Yang, Q. Xu, X. Ke, M. Liu, L.B. Qu, X. Chen, L. Mi, Constructing synergistic triazine and acetylene cores in fully conjugated covalent organic frameworks for cascade photocatalytic H₂O₂ production, *Chem. Mater.* 34 (2022) 5232–5240.
- [138] M. Kou, Y. Wang, Y. Xu, L. Ye, Y. Huang, B. Jia, H. Li, J. Ren, Y. Deng, J. Chen, Y. Zhou, K. Lei, L. Wang, W. Liu, H. Huang, T. Ma, Molecularly engineered covalent organic frameworks for hydrogen peroxide photosynthesis, *Angew. Chem. Int. Ed.* 61 (2022), e202200413.
- [139] H. Wang, C. Yang, F. Chen, G. Zheng, Q. Han, A crystalline partially fluorinated triazine covalent organic framework for efficient photosynthesis of hydrogen peroxide, *Angew. Chem. Int. Ed.* 61 (2022), e202202328.
- [140] S. Chai, X. Chen, X. Zhang, Y. Fang, R.S. Sprick, X. Chen, Rational design of covalent organic frameworks for efficient photocatalytic hydrogen peroxide production, *Environ. Sci.: Nano* 9 (2022) 2464–2469.
- [141] F. Liu, P. Zhou, Y. Hou, H. Tan, Y. Liang, J. Liang, Q. Zhang, S. Guo, M. Tong, J. Ni, Covalent organic frameworks for direct photosynthesis of hydrogen peroxide from water, air and sunlight, *Nat. Commun.* 14 (2023) 4344.
- [142] D. Chen, W. Chen, Y. Wu, L. Wang, X. Wu, H. Xu, L. Chen, Covalent organic frameworks containing dual O₂ reduction centers for overall photosynthetic hydrogen peroxide production, *Angew. Chem. Int. Ed.* 62 (2023), e202217479.
- [143] F. Tan, Y. Zheng, Z. Zhou, H. Wang, X. Dong, J. Yang, Z. Ou, H. Qi, W. Liu, Z. Zheng, X. Chen, Aqueous synthesis of covalent organic frameworks as photocatalysts for hydrogen peroxide production, *CCS Chem.* 4 (2022) 3751–3761.
- [144] J.N. Chang, Q. Li, J.W. Shi, M. Zhang, L. Zhang, S. Li, Y. Chen, S.L. Li, Y.Q. Lan, Oxidation-reduction molecular junction covalent organic frameworks for full reaction photosynthesis of H₂O₂, *Angew. Chem. Int. Ed.* 62 (2023), e202218868.
- [145] M. Liu, L. Guo, S. Jin, B. Tan, Covalent triazine frameworks: synthesis and applications, *J. Mater. Chem. A* 7 (2019) 5153–5172.
- [146] N. Tahir, C. Krishnaraj, K. Leus, P.V.D. Voort, Development of covalent triazine frameworks as heterogeneous catalytic supports, *Polymers* 11 (2019) 1326.
- [147] P. Kuhn, M. Antonietti, A. Thomas, Porous, covalent triazine-based frameworks prepared by ionothermal synthesis, *Angew. Chem. Int. Ed.* 47 (2008) 3450–3453.
- [148] L. Chen, L. Wang, Y. Wan, Y. Zhang, Z. Qi, X. Wu, H. Xu, Acetylene and diacetylene functionalized covalent triazine frameworks as metal-free photocatalysts for hydrogen peroxide production: A new two-electron water oxidation pathway, *Adv. Mater.* 32 (2020) 1904433.
- [149] X. Yu, B. Viengkeo, Q. He, X. Zhao, Q. Huang, P. Li, W. Huang, Y. Li, Electronic tuning of covalent triazine framework nanoshells for highly efficient photocatalytic H₂O₂ production, *Adv. Sustain. Syst.* 5 (2021) 2100184.
- [150] H. Cheng, H. Lv, J. Cheng, L. Wang, X. Wu, H. Xu, Rational design of covalent heptazine frameworks with spatially separated redox centers for high-efficiency photocatalytic hydrogen peroxide production, *Adv. Mater.* 34 (2022) 2107480.
- [151] C. Wu, Z. Teng, C. Yang, F. Chen, H.B. Yang, L. Wang, H. Xu, B. Liu, G. Zheng, Q. Han, Polarization engineering of covalent triazine frameworks for highly efficient photosynthesis of hydrogen peroxide from molecular oxygen and water, *Adv. Mater.* 34 (2022) 2110266.
- [152] Y. Zheng, T. Gao, S. Chen, C.T.J. Ferguson, K.A.I. Zhang, F. Fang, Y. Shen, N. A. Khan, L. Wang, L. Ye, CsPbBr₃ quantum dots-decorated porous covalent triazine frameworks nanocomposites for enhanced solar-driven H₂O₂ production, *Compos. Commun.* 36 (2022), 101390.
- [153] W. Ren, Q. Chang, N. Li, J. Yang, S. Hu, Carbon dots-modulated covalent triazine frameworks with exceptionally rapid hydrogen peroxide production in water, *Chem. Eng. J.* 451 (2023), 139035.
- [154] J.S.M. Lee, A.I. Cooper, Advances in conjugated microporous polymers, *Chem. Rev.* 120 (2020) 2171–2214.
- [155] X. Xu, Z. Li, Y. Sui, W. Huang, W. Chen, X. Li, D. Liu, Y. Li, F. Deng, G. Zhou, L. Zhong, H. Zhong, Solvent-induced flower- and cudgel-shaped porous organic polymers: effective supports of palladium nanoparticles for dehalogenation in net water, *ChemNanoMat* 8 (2022), e202100484.
- [156] Z. Fu, X. Wang, A. Gardner, X. Wang, S.Y. Chong, G. Neri, A.J. Cowan, L. Liu, X. Li, A. Vogel, R. Clowes, M. Bilton, L. Chen, R.S. Sprick, A.I. Cooper, A stable covalent organic framework for photocatalytic carbon dioxide reduction, *Chem. Sci.* 11 (2020) 543–550.
- [157] X.C. Li, Y. Zhang, C.Y. Wang, Y. Wan, W.Y. Lai, H. Pang, W. Huang, Redox-active triazatruxene-based conjugated microporous polymers for high-performance supercapacitors, *Chem. Sci.* 8 (2017) 2959–2965.
- [158] J.X. Jiang, F. Su, A. Trewin, C.D. Wood, N.L. Campbell, H. Niu, C. Dickinson, A. Y. Ganin, M.J. Rosseinsky, Y.Z. Khimyak, A.I. Cooper, Conjugated microporous poly(aryleneethynylene) networks, *Angew. Chem. Int. Ed.* 46 (2007) 8574–8578.
- [159] Z.J. Wang, S. Ghasimi, K. Landfester, K.A.I. Zhang, Photocatalytic suzuki coupling reaction using conjugated microporous polymer with immobilized palladium nanoparticles under visible light, *Chem. Mater.* 27 (2015) 1921–1924.
- [160] X. Xu, Y. Sui, W. Huang, W. Chen, X. Li, Y. Li, G. Wang, H. Ye, H. Zhong, Upgraded heterogenization of homogeneous catalytic systems by hollow porous organic frameworks with hierarchical porous shell for efficient carbon dioxide conversion, *Asian J. Org. Chem.* 11 (2022), e202100727.
- [161] Z.S. Wu, L. Chen, J. Liu, K. Parvez, H. Liang, J. Shu, H. Sachdev, R. Graf, X. Feng, K. Müllen, High-performance electrocatalysts for oxygen reduction derived from cobalt porphyrin-based conjugated mesoporous polymers, *Adv. Mater.* 26 (2014) 1450–1455.
- [162] Y. Liao, H. Wang, M. Zhu, A. Thomas, Efficient supercapacitor energy storage using conjugated microporous polymer networks synthesized from buckwald-hartwig coupling, *Adv. Mater.* 30 (2018) 1705710.
- [163] Y. Zhang, S. A, Y. Zou, X. Luo, Z. Li, H. Xia, X. Liu, Y. Mu, Gas uptake, molecular sensing and organocatalytic performances of a multifunctional carbazole-based conjugated microporous polymer, *J. Mater. Chem. A* 2 (2014) 13422–13430.
- [164] X. Xu, H. Zhong, W. Huang, Y. Sui, R. Sa, W. Chen, G. Zhou, X. Li, D. Li, M. Wen, B. Jiang, The construction of conjugated organic polymers containing phenanthrenequinone redox centers for visible-light-driven H₂O₂ production from H₂O and O₂ without any additives, *Chem. Eng. J.* 454 (2023), 139929.

- [165] H. Yan, M. Shen, Y. Shen, X.D. Wang, W. Lin, J. Pan, J. He, Y.X. Ye, X. Yang, F. Zhu, J. Xu, J. He, G. Ouyang, Spontaneous exciton dissociation in organic photocatalyst under ambient conditions for highly efficient synthesis of hydrogen peroxide, *PNAS* 119 (2022), e2202913119.
- [166] K. Oka, H. Nishide, B. Winther-Jensen, Copolymer of phenylene and thiophene toward a visible-light-driven photocatalytic oxygen reduction to hydrogen peroxide, *Adv. Sci.* 8 (2021) 2003077.
- [167] C. Yang, S. Wan, B. Zhu, J. Yu, S. Cao, Calcination-regulated microstructures of donor-acceptor polymers towards enhanced and stable photocatalytic H_2O_2 production in pure water, *Angew. Chem. Int. Ed.* 61 (2022), e202208438.
- [168] S. Kumar, V.R. Battula, N. Sharma, S. Samanta, B. Rawat, K. Kailasam, A metal-free heptazine-porphyrin based porous polymeric network as an artificial leaf for carbon free solar fuels, *J. Mater. Chem. A* 10 (2022) 14568–14575.
- [169] S. Wang, G. Kumar, H. Tian, Organic polymer dots based on star-shaped truxene-core polymers for photocatalytic H_2O_2 production, *Sol. RRL* 6 (2022) 2200755.
- [170] L. Liu, M.Y. Gao, H. Yang, X. Wang, X. Li, A.I. Cooper, Linear conjugated polymers for solar-driven hydrogen peroxide production: The importance of catalyststability, *J. Am. Chem. Soc.* 143 (2021) 19287–19293.
- [171] Y.X. Ye, J. Pan, Y. Shen, M. Shen, H. Yan, J. He, X. Yang, F. Zhu, J. Xu, J. He, G. Ouyang, A solar-to-chemical conversion efficiency up to 0.26% achieved in ambient conditions, *PNAS* 118 (2021), e2115666118.
- [172] X. Xu, R. Sa, W. Huang, Y. Sui, W. Chen, G. Zhou, X. Li, Y. Li, H. Zhong, Conjugated organic polymers with anthraquinone redox centers for efficient photocatalytic hydrogen peroxide production from water and oxygen under visible light irradiation without any additives, *ACS Catal.* 12 (2022) 12954–12963.
- [173] X. Xu, Y. Sui, W. Chen, G. Zhou, Y. Li, H. Zhong, H.R. Wen, Anthraquinone-based conjugated organic polymers containing dual oxidation centers for photocatalytic H_2O_2 production from H_2O and O_2 under visible-light irradiation, *ACS Appl. Polym. Mater.* 5 (2023) 7571–7580.